Covalent Post-Assembly Modification of π-Conjugated Supramolecular Polymers Delivers Structurally Robust Light-Harvesting Nanoscale Objects

Victor Paulino,[a]† Kaixuan Liu,[a]† Valentino Cesiliano,[a] Ifigeneia Tsironi,[a] Arindam Mukhopadhyay,[a] Maria Kaufman,[a] Jean-Hubert Olivier[a]

[a] Department of Chemistry, University of Miami, Cox Science Center, 1301 Memorial Drive, Coral Gables, Florida 33146, United States

*Corresponding author: Jean-Hubert Olivier; E-mail: jh.olivier@miami.edu. Telephone: +1 305 284 3279

† These authors contributed equally

Table of Contents

1. **Materials and Instrumentation (p. 2)**
2. **Synthetic Procedures (p. 3-8)**
3. **FTIR Characterization of the Stapled Assemblies (p. 9-10)**
4. **Supramolecular Polymerization Mechanism (p. 11-13)**
5. **Gel Permeation Chromatography (p. 14-16)**
6. **Microscopy Characterization (p. 17-25)**
7. **Calculation of the Free-Exciton Bandwidth (Ex_{BW}) and Nearest Neighbor Excitonic Coupling (J_{12}) (p. 26-36)**
8. **Photoluminescence experiments (p. 37-39)**
9. **DFT Calculations and XYZ coordinates (p. 40-46)**
10. **^{1}H NMR, ^{13}C NMR, ESI and FTIR Spectra (p. 47-59)**
11. **References (p. 55)**

1. Materials and Instrumentation

Unless otherwise noted, all chemicals were used as received. Air-sensitive compounds were handled in Braun Labmaster DP glove box. Standard Schlenk techniques were employed to manipulate air sensitive solutions. Deuterated solvents employed for preparing solutions for NMR spectral acquisition were used as received from Cambridge Isotope Laboratories, Inc. Flash column chromatography was performed on the bench top, using silica gel (VWR, 70-90 μm). Anhyd $CuSO_4$ (Acros Organics), perylene-3,4,9,10-tetracarboxylic dianhydride (Acros Organics), sodium L-ascorbate (TCI Chemicals), etc. were used as received without any further purification. Compounds, N,N-Dimethylaminoethylamine, 2-bromoethanol, 4-pentyn-1-ol, *p*-toluenesulfonyl chloride, and DMAC were purchased from Tokyo Chemical Industry and used without further purification. Propargyl alcohol, tetraethylene glycol, polyethylene glycol, sodium hydride and sodium azide were purchased from Alfa Aesar without further purification. **PDA-Br$_2$,**[1] **N$_3$(EO)$_{13\pm5}$ N$_3$,**[2] and **N$_3$(EO)$_3$N$_3$**[3] were synthesized according to our previous work. PBS tablets were purchased from VWR where each tablet, when dissolved in 100 mL of water, prepares 1X PBS solution containing 137 mM sodium chloride, 2.7 mM potassium chloride, and 10 mM phosphate buffer.

All solvents employed for synthesis (HPLC grade) and purification (ACS grade) were purchased from VWR; they were, namely, tetrahydrofuran (THF), dichloromethane (DCM), acetonitrile (MeCN), methanol (MeOH), ethanol (EtOH), water, etc. Anhyd THF was prepared by distillation over Na/benzophenone under Argon. DCM, MeCN, and N,N-diisopropylethylamine, i.e., Hünig's base (Sigma-Aldrich) were dehydrated by distillation over anhyd calcium hydride (Strem Chemicals) under Ar and stored over activated molecular sieves in Schlenk round bottom flasks prior to using. NMR spectra were recorded on Avance Bruker spectrometers (400 and 500 MHz). UV-vis-NIR spectra were recorded on a Cary 5000 equipped with a Peltier-controlled heating stage (Versa 20 from Quantum Northwest). IR spectra were recorded on a Perkin Elmer Frontier FTIR. Mass spectra were obtained on a MicroQ-TOF ESI mass spectrometer. Silicon wafers (single side polished; orientation <111>, P-type with boron as the dopant) were purchased from University Wafer. The tethered assemblies were analyzed using a GE/ÄKTA pure 25 gel permeation chromatography system (GE Healthcare Bio-Science AB, Björkgatan, Uppsala, Sweden) equipped with one preparative column (160 x 16 mm; stationary phase: sephacryl S-200). The GPC system uses a three-wavelength detection (490 nm, 260 nm, 540 nm) system. Simulations and curve fittings were executed using Matlab 9.7.0 R2019 update 5.v. Fluorescence measurements were collected using a Shimadzu RF-6000 Spectro Fluorophotometer.

2. Synthetic Procedures

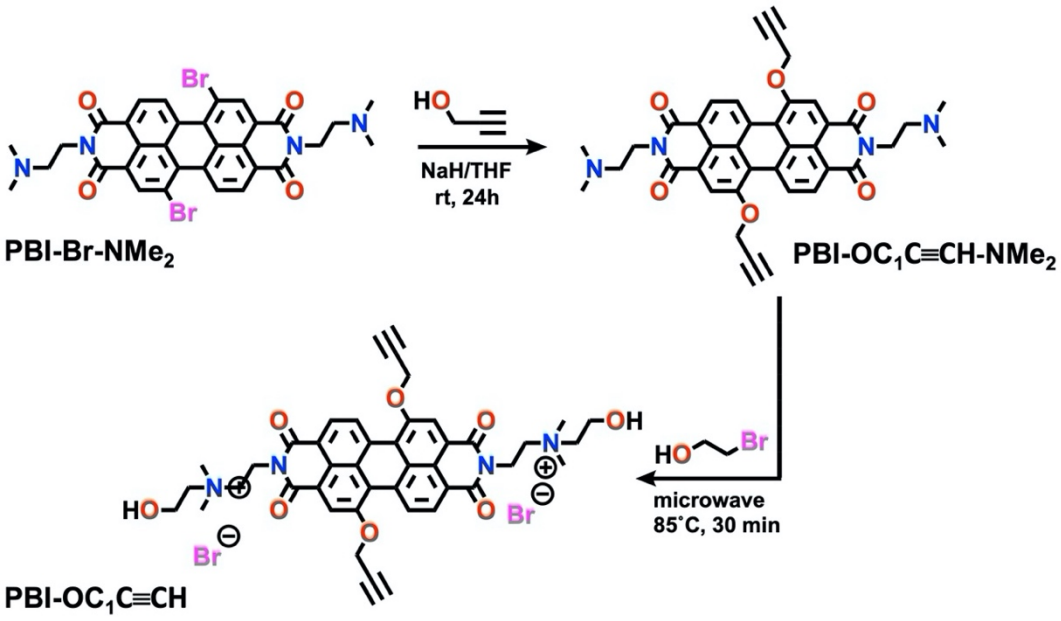

Scheme S1. Synthesis of **PBI-OC$_1$C≡CH**.

PBI-OC$_1$C≡CH-NMe$_2$. A solution of propargyl alcohol (0.17 g, 2.9 mmol) dissolved in 15 to 20 mL of distilled THF was added dropwise to a flask under argon containing NaH (76 mg of 57%, 1.7 mmol). The mixture was stirred for 20 min at room temperature, and a solution of **PDI-Br-NMe$_2$** (0.25 g, 0.36 mmol) in 80 mL of dry THF was added dropwise over a 10-min period. The mixture was stirred for 24 h under argon at room temperature, and the solvent was removed under reduced pressure. The solid was washed with a small amount of MeCN to remove any unreacted propargyl alcohol. The crude product was purified by column chromatography over deactivated silica gel (dichloromethane/methanol/trimethylamine from 97:2:1 to 91:8:1). After removal of the solvent under reduced pressure, the compound was obtained as a violet solid (0.19 g, 82%).

Characterization data of **PBI-OC$_1$C≡CH-NMe$_2$**. ^{1}H NMR (400 MHz, $CDCl_3$) δ = 9.48 (d, J = 8.3 Hz, 2H), 8.53 (d, J = 8.4 Hz, 2H),), 8.49 (s, 2H), 5.15 (d, J = 2.3 Hz, 4H), 4.37 (t, J = 6.9 Hz, 4H), 2.77 (t, J = 6.9 Hz, 4H), 2.70 (t, J = 2.3 Hz, 2H), 2.42 (s, 12H); ESI-MS$^+$ m/z Calcd for $C_{38}H_{33}N_4O_6^{2+}$ 641.2400 $[M+H]^+$, found 642.2467, $C_{38}H_{34}N_4O_6^{2+}$ 321.1239 $[M+2H]^{2+}$, found 321.6276. FT-IR: $\bar{\upsilon}$ = 3267, 2940, 2676, 2123, 1690, 1648, 1589, 1332, 1269 cm^{-1}. Please note that long acquisition times are needed on account of poor solubility of **PBI-OC$_1$C≡CH-NMe$_2$** in $CDCl_3$ or other organic solvents. This limitation prevented the acquisition of a ^{13}C NMR spectrum.

PBI-OC$_1$C≡CH. **PBI-OC$_1$C≡CH-NMe$_2$** (47 mg. 0.07 mmol) was added into bromoethanol (5 mL, 71 mmol) followed by the addition of DIPEA (0.5 mL, 2.9 mmol). The reaction was heated under microwave irradiation at 85 °C for 0.5 h. After cooling down to rt, the mixture was precipitated in THF (30 mL). The solid was filtered by glass frit and washed with THF (50 mL) to remove any unreacted starting materials. The solvent was removed under reduced pressure yielding a dark purple solid (42 mg, 63%)

Characterization data of **PBI-OC$_1$C≡CH**. ^{1}H NMR (400 MHz, d_6-DMSO) δ = 9.48 (d, J = 8.9 Hz, 2H), 8.53 (s, 2H), 8.43 (d, J = 8.2 Hz, 2H), 5.45 (s, 4H), 5.39 (t, J = 4.1 Hz, 2H), 4.53 (br, s, 4H), 3.96 (br, s, 4H), 3.84 (s, 2H), 3.76 – 3.70 (m, 4H), 3.66 – 3.60 (m, 4H), 3.30 (s, 12H); ^{13}C NMR (101 MHz, d_6-DMSO) δ = 163.16, 163.05, 155.51, 133.20, 129.34, 129.17, 128.74, 123.29, 121.57, 121.54, 118.73, 80.55, 78.75, 65.74, 60.86, 57.96, 55.46, 51.87. ESI-MS$^+$ m/z Calcd for $C_{42}H_{42}N_4O_8^{2+}$ 365.1502 $[M]^{2+}$, found 365.1470. FT-IR: $\bar{\upsilon}$ = 3239, 3015, 2123, 1690, 1646, 1589, 1331, 1270 cm^{-1}.

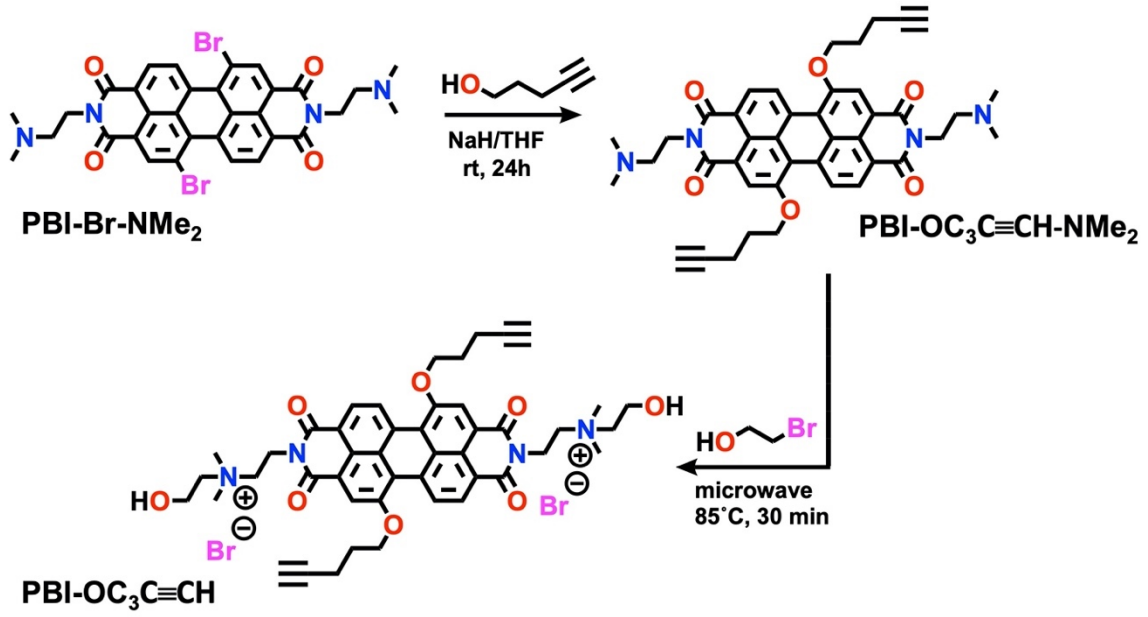

Scheme S2. Synthesis of **PBI-OC$_3$C≡CH**.

PBI-OC$_3$C≡CH-NMe$_2$. A solution of 4-pentyn-1-ol (0.23 g, 2.8 mmol) dissolved in 15 to 20 mL of distilled THF was added dropwise to a flask under argon containing NaH (73 mg of 57%, 1.7 mmol). The mixture was stirred for 20 min at rt, and a solution of **PDI-Br-NMe$_2$** (0.24 g, 0.35 mmol) dissolved in 80 mL dry THF was added dropwise over a 10 min period. The mixture was stirred for 24 h under argon at rt, and the solvent was removed under reduced pressure. The solid was washed with small amount of MeCN to remove any excess of unreacted 4-Pentyn-1-ol. The crude product was purified by column chromatography over deactivated silica gel (dichloromethane/methanol/trimethylamine

from 97:2:1 to 91:8:1). After removal of the solvent under reduced pressure, the compound was obtained as a violet solid (0.15 g, 60%).

Characterization data of **PBI-OC$_3$C≡CH-NMe$_2$**. FT-IR: $\bar{\upsilon}$ = 3260, 2777, 2112, 1690, 1649, 1596, 1334, 1268 cm^{-1}. ^{1}H NMR (400 MHz, $CDCl_3$) δ = 9.40 (d, J = 8.5 Hz, 2H), 8.46 (d, J = 8.4 Hz, 2H),), 8.32 (s, 2H), 4.53 (t, J = 6.2 Hz, 4H), 4.35 (t, J = 7.0 Hz, 4H), 2.75 (t, J = 6.7 Hz, 4H), 2.57 – 2.49 (m, 4H), 2.35 (s, 12H), 2.28 – 2.22 (m, 4H), 2.07 (s, 2H). ESI-MS$^+$ m/z Calcd for $C_{42}H_{41}N_4O_6^{2+}$ 697.3026 $[M+H]^+$, found 697.3017, $C_{42}H_{42}N_4O_6^{2+}$ 349.1552 $[M+2H]^{2+}$, found 349.1538. FT-IR: $\bar{\upsilon}$ = 3260, 2777, 2112, 1690, 1649, 1596, 1334, 1268 cm^{-1}. Please note that long acquisition times are needed on account of poor solubility of **PBI-OC$_3$C≡CH-NMe$_2$** in $CDCl_3$ or other organic solvents. This limitation prevented the acquisition of a ^{13}C NMR spectrum.

PBI-OC$_3$C≡CH. **PBI-OC$_3$C≡CH-NMe$_2$** (30 mg. 0.04 mmol) was dissolved in bromoethanol (5 mL, 71 mmol) followed by addition of DIPEA (1 mL, 2.9 mmol). The reaction was heated under microwave irradiation at 90 °C for 0.5 h. After cooling down to rt, the mixture was precipitated in THF (30 mL). The solid was filtered over a glass frit and washed with THF (50 mL). The solvent was removed under reduced pressure yielding a dark purple solid (19 mg, 46%)

Characterization data of **PBI-OC$_3$C≡CH**. ^{1}H NMR (400 MHz, d_6-DMSO) δ = 9.55 (br, s, 2H), 8.56 (br, s, 2H), 8.41 (br, s, 2H), 5.38 (br, s, 2H), 4.61 – 4.54 (m, 8H), 3.96 (br, s, 4H), 3.73 (br, s, 4H), 3.61 (br, s, 4H), 2.90 (s, 2H), 2.24 (br, s, 4H). ESI-MS$^+$ m/z Calcd for $C_{46}H_{50}N_4O_8^{2+}$ 393.1815 $[M]^{2+}$, found 393.1820. FT-IR: $\bar{\upsilon}$ = 3270, 2922, 2112, 1690, 1648, 1589, 1333, 1270 cm^{-1}. Please note that long acquisition times are needed on account of poor solubility of **PBI-OC$_3$C≡CH** in d_6-DMSO or other organic solvents. This limitation prevented the acquisition of a ^{13}C NMR spectrum.

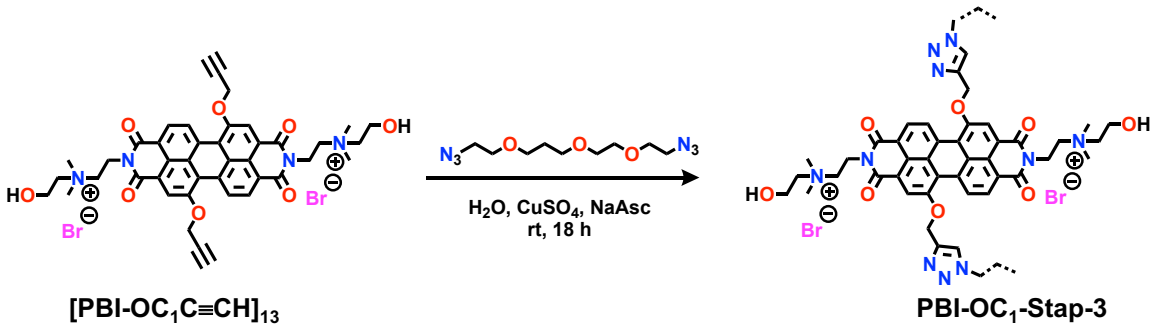

Scheme S3. Synthesis of the stapled assembly **PBI-OC$_1$-Stap-3**.

Stapled Assembly PBI-OC$_1$-Stap-3: To a solution of **[PBI-OC$_1$C≡CH]$_{13}$** (6.5 mg, 7.3 µmol) and **N$_3$(EO)$_3$N$_3$** (2.14 mg, 8.8 µmol) in degassed HPLC water (6.3 mL), a solution of $CuSO_4$ (0.12 mg, 1 µmol) and sodium ascorbate (0.36 mg, 1.8 µmol) in degassed HPLC

water (1 mL) is added. The solution is stirred at room temperature for 18 hours under argon. The reaction mixture is centrifuged in a 5000 sartorius MWCO centrifuge filter at 3900 rpm for 20 minutes repeatedly until the filtrate becomes clear. The solution is then purified on a Sephacryl 200HR size exclusion column using a buffer solution (30% CH_3CN in H_2O, 1 eq. PBS). The buffer solution is desalted and concentrated by centrifuging in a 5000 Sartorius MWCO centrifuge filter at 6000 rpm for 20 minutes with HPLC grade water around 10 times, yielding a solution of **PBI-OC$_1$-Stap-3** in water. The suspended **PBI-OC$_1$-Stap-3** is stable and can be dried by evaporating water to form a dark purple, solid. IR (neat solid): $\bar{\upsilon}$ = 3325, 2919, 1691, 1651, 1590, 1411, 1334, 1271 cm^{-1}. Retention time: 23.72 min, 11,600 g mol^{-1}. Vis (solvent, λ_{max} (cm^{-1}), log ε): H_2O, 18484, 4.364; DMF, 18640, 4.300.

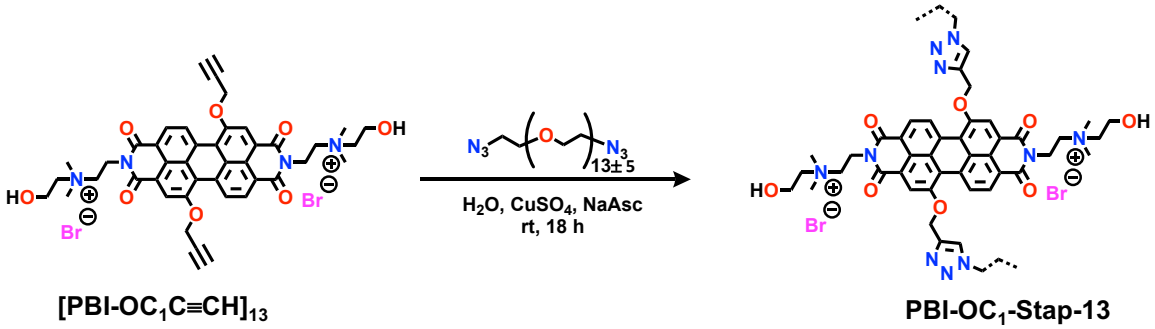

Scheme S4. Synthesis of the stapled assembly **PBI-OC$_1$-Stap-13**.

Stapled Assembly PBI-OC$_1$-Stap-13: To a solution of **[PBI-OC$_1$C≡CH]$_{13}$** (8.9 mg, 10 µmol) and **N$_3$(EO)$_{13}$N$_3$** (7.7 mg, 12 µmol) in degassed HPLC water (9 mL), a solution of $CuSO_4$ (0.16 mg, 1 µmol) and sodium ascorbate (0.4 mg, 2 µmol) in degassed HPLC water (1mL) is added. The solution is stirred at room temperature overnight under Argon. The reaction mixture is centrifuged in a 5000 Sartorius MWCO centrifuge filter at 6000 rpm for 20 minutes repeatedly until filtrate becomes clear. The solution is then purified on a Sephacryl 200HR size exclusion column using a buffer solution (30% CH_3CN in H_2O, 1 eq. PBS). The buffer solution is desalted and concentrated by centrifuging in a 5000 Sartorius MWCO centrifuge filter at 6000 rpm for 20 minutes with HPLC grade water round 10 times, yielding a solution of **PBI-OC$_1$-Stap-13** in water. The suspended **PBI-OC$_1$-Stap-13** is stable and can be dried by evaporating water to form a dark purple, solid. IR (neat solid): $\bar{\upsilon}$ = 3304, 2867, 1690, 1649, 1589, 1460, 1413, 1336, 1272, 1084. Retention time: 22.09 min, 17,600 g mol^{-1}. Vis (solvent, λ_{max} (cm^{-1}), log ε): H_2O, 18459, 4.388; DMF, 18572, 4.313.

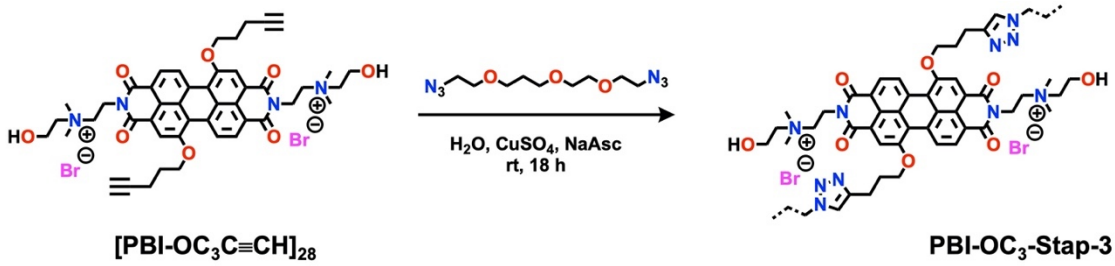

Scheme S5. Synthesis of the stapled assembly **PBI-OC$_3$-Stap-3**.

Stapled Assembly PBI-OC$_3$-Stap-3: To a solution of **[PBI-OC$_3$C≡CH]$_{28}$** (8.5 mg, 9 µmol) and **N$_3$(EO)$_3$N$_3$** (2.6 mg, 10.8 µmol) in degassed HPLC water (8 mL), a solution of $CuSO_4$ (0.15 mg, 1 µmol) and sodium ascorbate (0.4 mg, 2 µmol) in degassed HPLC water (1mL) is added. The solution is stirred at room temperature overnight under argon. The reaction mixture is centrifuged in a 5000 Sartorius MWCO centrifuge filter at 6000 rpm for 20 minutes repeatedly until the filtrate becomes clear. The solution is then purified on a Sephacryl 200HR size exclusion column using a buffer solution (30% CH_3CN in H_2O, 1 eq. PBS). The buffer solution is desalted and concentrated by centrifuging in a 5000 sartorious MWCO centrifuge filter at 6000 rpm for 20 minutes with HPLC grade water round 10 times, yielding a solution of **PBI-OC$_3$-Stap-3** in water. The suspended **PBI-OC$_3$-Stap-3** is stable and can be dried by evaporating water to form a dark purple, solid. IR (neat solid): $\bar{\upsilon}$ = 3292, 2929, 2866, 1691, 1650, 1590, 1414, 1334, 1271, 1215, 1196, 1036. Retention time: 22.97 min, 14,850 g mol^{-1}. Vis (solvent, λ_{max} (cm^{-1}), log ε): H_2O, 18418, 4.4267; DMF, 18597, 4.400.

Scheme S6. Synthesis of the stapled assembly **PBI-OC$_3$-Stap-13**.

Stapled Assembly PBI-OC$_3$-Stap-13: To a solution of **[PBI-OC$_3$C≡CH]$_{28}$** (9.3 mg, 9.8 µmol) and **N$_3$(EO)$_{13}$N$_3$** (7.52 mg, 11.7 µmol) in degassed HPLC water (8.8 mL), a solution of $CuSO_4$ (0.16 mg, 1 µmol) and sodium ascorbate (0.4 mg, 2 µmol) in degassed HPLC water (1mL) is added. The solution is stirred at room temperature overnight under argon. The reaction mixture is centrifuged in a 5000 Sartorius MWCO centrifuge filter at 6000 rpm for 20 minutes repeatedly until filtrate becomes clear. The solution is then purified on a Sephacryl 200HR size exclusion column using a buffer solution (30% CH_3CN in H_2O, 1 eq.

PBS). The buffer solution is desalted and concentrated by centrifuging in a 5000 Sartorious MWCO centrifuge filter at 6000 rpm for 20 minutes with HPLC grade water round 10 times, yielding a solution of **PBI-OC$_3$-Stap-13** in water. The suspended **PBI-OC$_3$-Stap-13** is stable and can be dried by evaporating water to form a dark purple, solid. IR (neat solid): $\bar{\upsilon}$ = 3302, 2939, 2870, 1692, 1651, 1592, 1415, 1337, 1272, 1215, 1199, 1085, 1045. Retention time: 20.83 min, 23,900 g mol^{-1}. Vis (solvent, λ_{max} (cm^{-1}), log ε): H_2O, 18397, 4.369; DMF, 18583, 4.363.

3. FTIR Characterization of the Tethered Assemblies

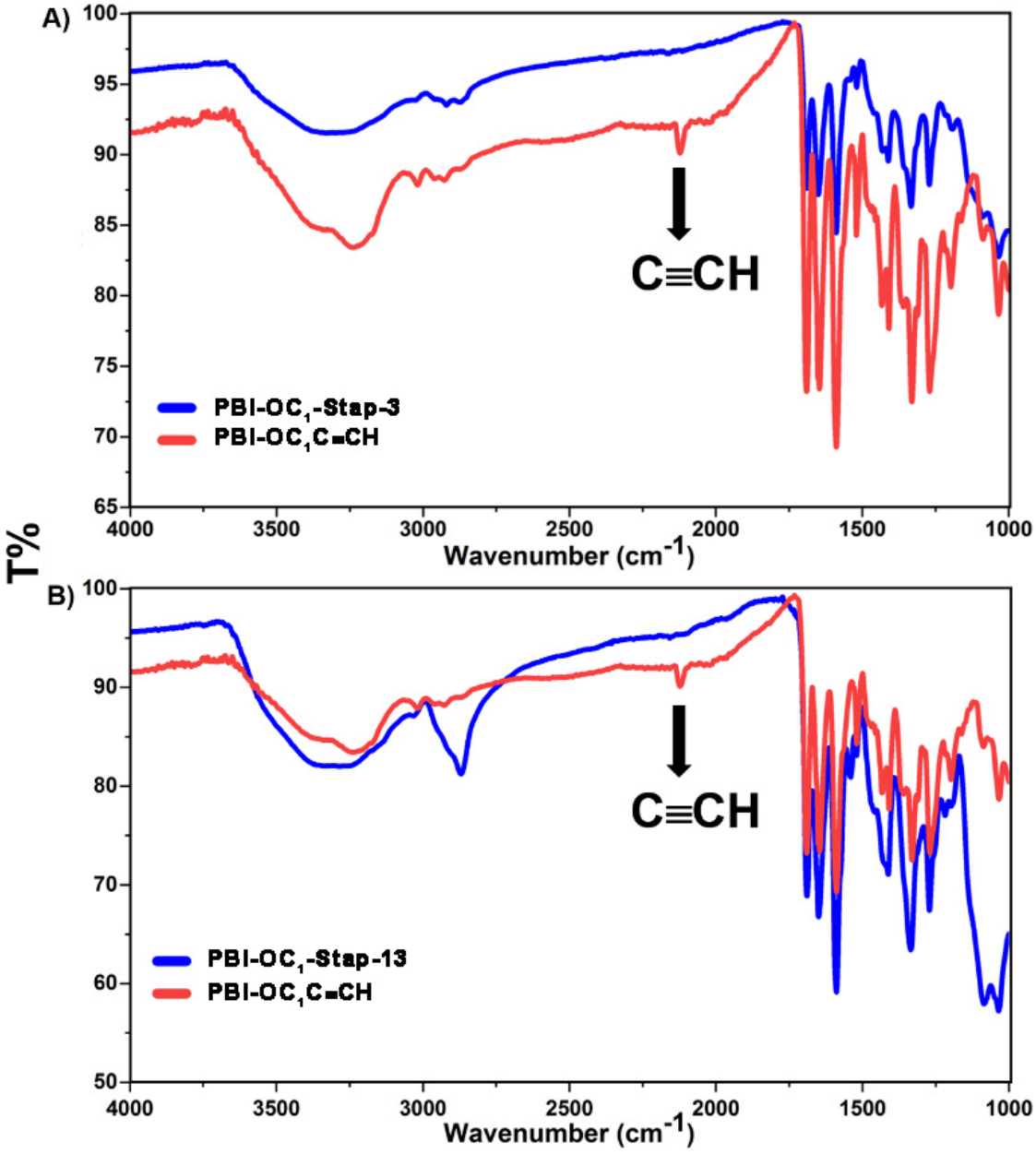

Figure S1. Fourier Transform Infrared spectra of the parent assembly **PBI-OC$_1$C≡CH**, and the stapled Superstructures **PBI-OC$_1$-Stap-3** (A) and **PBI-OC$_1$-Stap-13** (B).

To further confirm the formation of locked polymers, the original monomer **PBI-OC$_1$C≡CH**, post-assembly modified **PBI-OC$_1$-Stap-3** and **PBI-OC$_1$-Stap-13** were investigated by FTIR spectra. As evidenced in (A) and (B), the transmittance of **-C≡C-H** centered at 2123 cm^{-1} disappeared after "click" reaction suggesting the full conversion of the terminal alkyne groups.

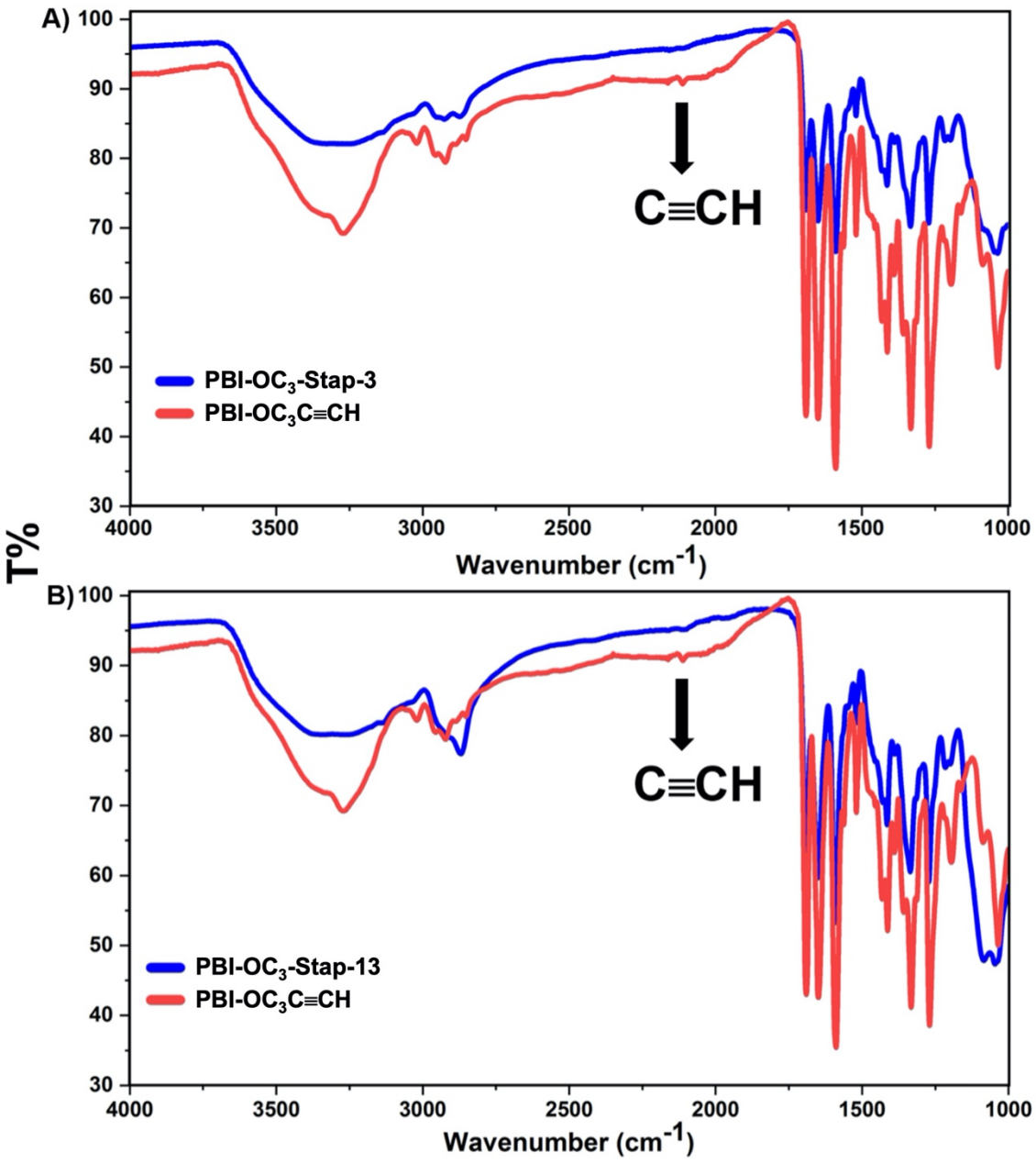

Figure S2. Fourier Transform Infrared spectra of the parent, unlock assembly **PBI-OC$_3$C≡CH**, and the locked superstructure **PBI-OC$_3$-Stap-3** (A) and **PBI-OC$_3$-Stap-13** (B).

To further confirm the formation of locked polymers, the original monomer **PBI-OC$_3$C≡CH**, post-assembly modified **PBI-OC$_3$-Stap-3** and **PBI-OC$_3$-Stap-13** were investigated by FTIR spectra. As evidenced in (A) and (B), the transmittance of **-C≡C-H** centered at 2112 cm^{-1} disappeared after "click" reaction suggesting the full conversion of the terminal alkyne groups.

4. Supramolecular Polymerization Mechanism

To elucidate the supramolecular polymerization mechanism that regulates the aggregation of the non-covalent building blocks, a solvent-dependent equilibrium model was exploited. We have previously used this approach on water-soluble PBI building blocks. The dimensionless mass balance equation (eq. S1) is used to express the degree of aggregation (eq. S2) as a function of the DMF solvent ratio (eq. S3).

$$x_{tot} = \sigma^{-1}\left(\frac{(\sigma x)^{n+1}(n\sigma x-n-1)}{(\sigma x-1)^2}+\frac{\sigma x}{(\sigma x-1)^2}\right)-\sigma^{n-1}\left(\frac{(x)^{n+1}(nx-n-1)}{(x-1)^2}\right) \text{ (eq. S1)}$$

$$\varphi = \left(\frac{x_{tot}-x}{x_{tot}}\right) \text{ (eq. S2)}$$

$$\Delta G = \Delta G^0 + m f \text{ (eq. S3)}$$

$$K_e = \exp(-\Delta G/R\ T) \text{ (eq. S4)}$$

In eq. S1, $x_{tot} = K_e[C_{tot}]$ and $x = K_e[M]$. In eq. S3 m is a correction factor that accounts for the change Gibbs free energy as a function of the solvent ratio (f).

Four parameters ΔG^0, σ, m, and p are used in the fitting procedure. A non-linear least square analysis is performed in Matlab (lsqnonlin) using the Levenberg-Marquardt algorithm. To find the parameters that fit the experimental data, a set of 500 different starting parameters is used and the non-linear least squared regression is performed. The starting parameters were generated using the lhsdesign function in Matlab and are bracketed by the following extrema:
ΔG^0 [-95,-15] kJ mol^{-1}, m [5,50] mol^{-1}, σ [0.1,1.2], p [0.5,1.2]. These boundaries were adjusted to find the best fitting parameters.

The fitting parameters were validated by calculating the denaturation curves using eq. S1, S2 and $k_e = \exp(-\Delta G/R\ T)$.

The monomer concentration as a function of DMF volume fraction is found via:

$$[C_{tot}] = \frac{[M]}{(1-Ke\ [M])^2} \text{ (eq. S5)}$$

A binary search algorithm is used to solved eq. S4 and is dependent on the DMF volume fraction via K_e.

The concentration of monomer comprised in the aggregate fraction is calculated via:

$$[Aggregate] = \frac{[M]}{(1-K_e\ [M])^2} - [M] \text{ (eq. S6)}$$

The degree of supramolecular polymerization DPN is estimated using:[4]

$$DP_N = \frac{1}{2} + \frac{1}{2}\sqrt{4K_e c_T + 1} \text{ (eq. S7)}$$

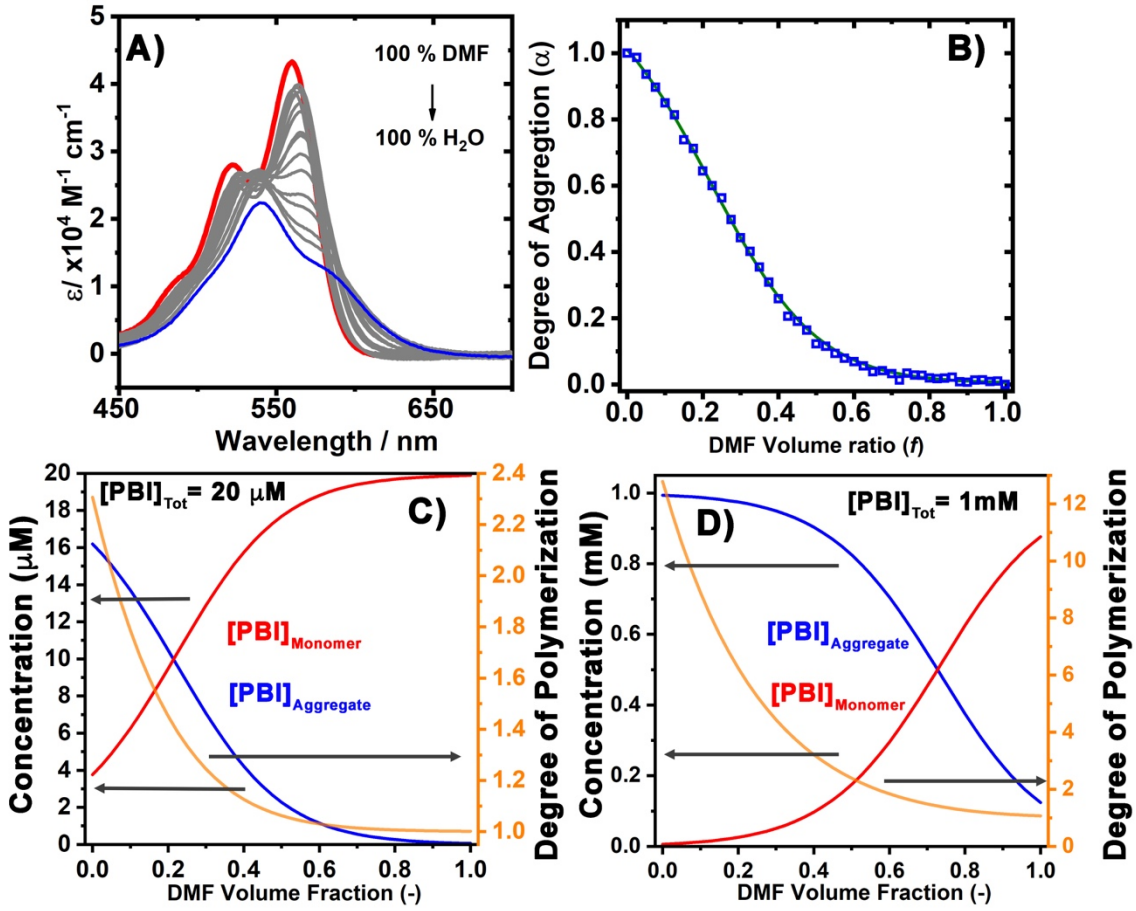

Figure S3. A) Solvent-dependent UV-vis spectra that chronicle the aggregation of a 20 mM solution of **PBI-OC$_1$C≡CH** as a function of the ratio of H_2O (bad solvent) in DMF (good solvent). B) Experimental degree of aggregation (open blue square) as a function of DMF Volume ratio (f) in water. An isodesmic equilibrium model (σ=1) best fit the experimental data. C-D) concentration of the free monomer ([PBI]monomer) and the monomers that exist in an aggregated state ([PBI]Aggregate) as a function of DMF volume fraction with $[PBI]_{Tot}$= 20 mM (C) and $[PBI]_{Tot}$= 1 mM.

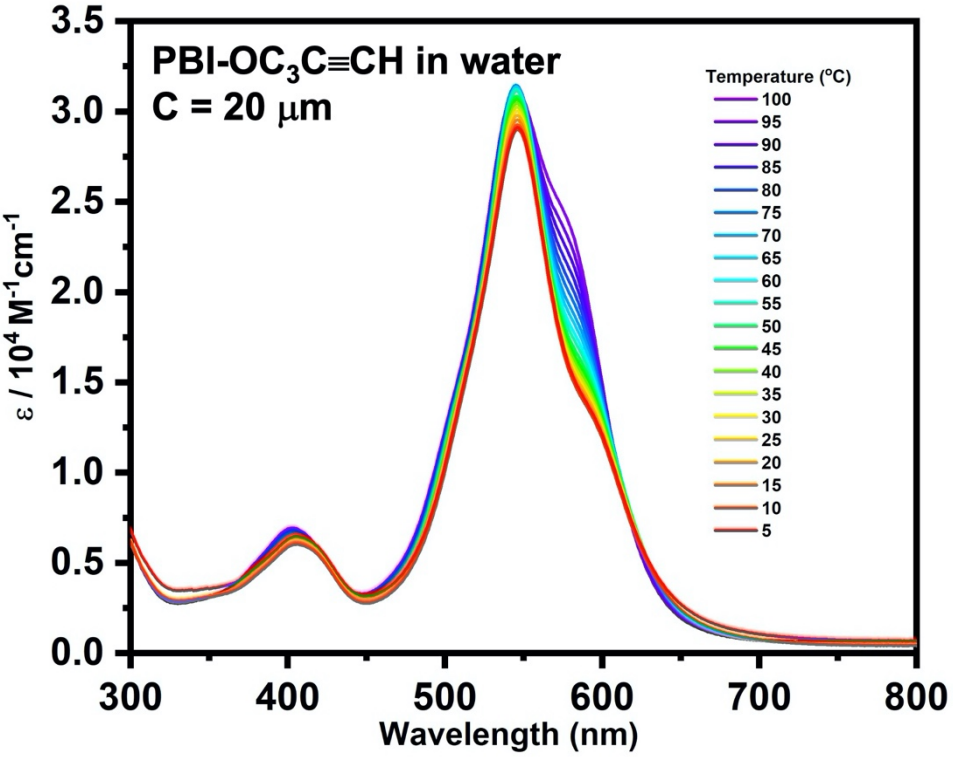

Figure S4. Temperature-dependent ground-state electronic absorption spectra recorded for the **PBI-OC$_3$C≡CH** building block in water. Although the ratio of the intensity of the 0-1 and 0-0 vibronic transitions evolved as a function of temperature, this building block remains aggregated at high temperatures. This behavior hampers elucidation the aggregation mechanism.

5. Gel Permeation Chromatography (GPC)

Please refer to our previous work for more details on the GPC characterization of stapled assemblies.[2, 5] Note that we calibrated the gel permeation chromatography column using a polystyrene sulfonate standard. The choice of this standard is solely based on the solvent buffer condition required to elute the **PBI-OC$_1$-Stap-3**, **PBI-OC$_1$-Stap-13**, **PBI-OC$_3$-Stap-3**, and **PBI-OC$_3$-Stap-13** stapled assemblies on the S-200 stationary phase. Using the calibration curve built from the elution of polystyrene sulfonate standard shown in Figure S5, the elution time of 22 min. corresponds to a molecular weight (M_W) of 5,200 Da on the dextran scale but 18,000 Da on the globular scale. It is important to note that any attempts to run the parent non-covalent assemblies **PBI-OC$_3$C≡CH** and **PBI-OC$_1$C≡CH** on S-200 Sephacryl using identical elution conditions were unsuccessful as the compounds remained adsorbed on the stationary phase.

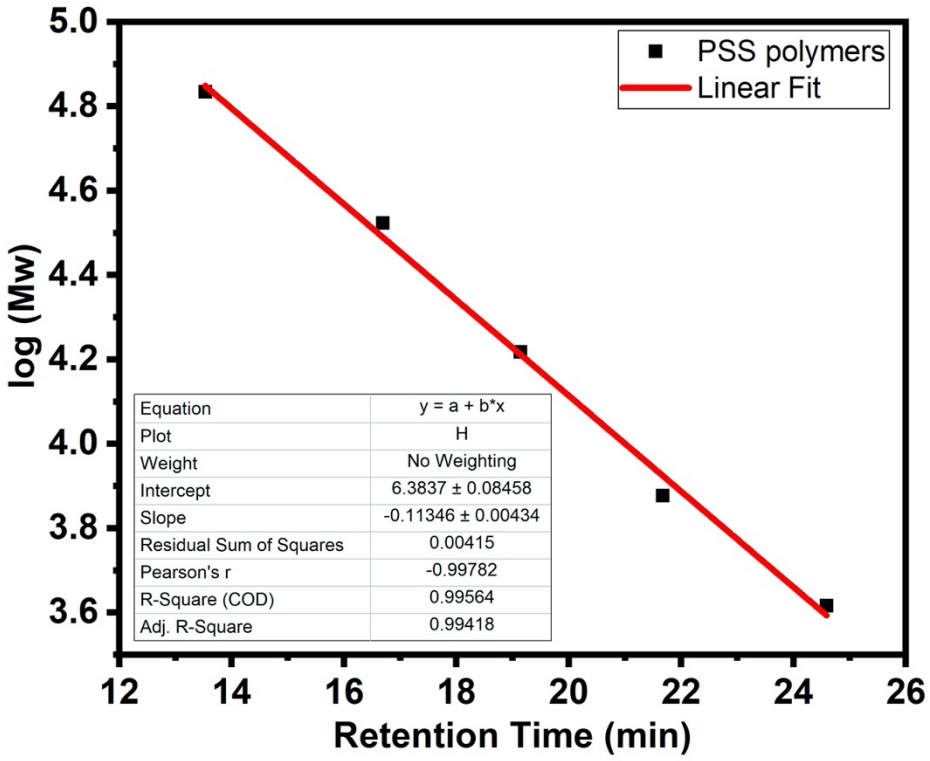

Figure S5. Elution time vs. the log of the molecular weight of the polystyrene sulfonate standard passed through a Sephacryl 200HR size exclusion column.

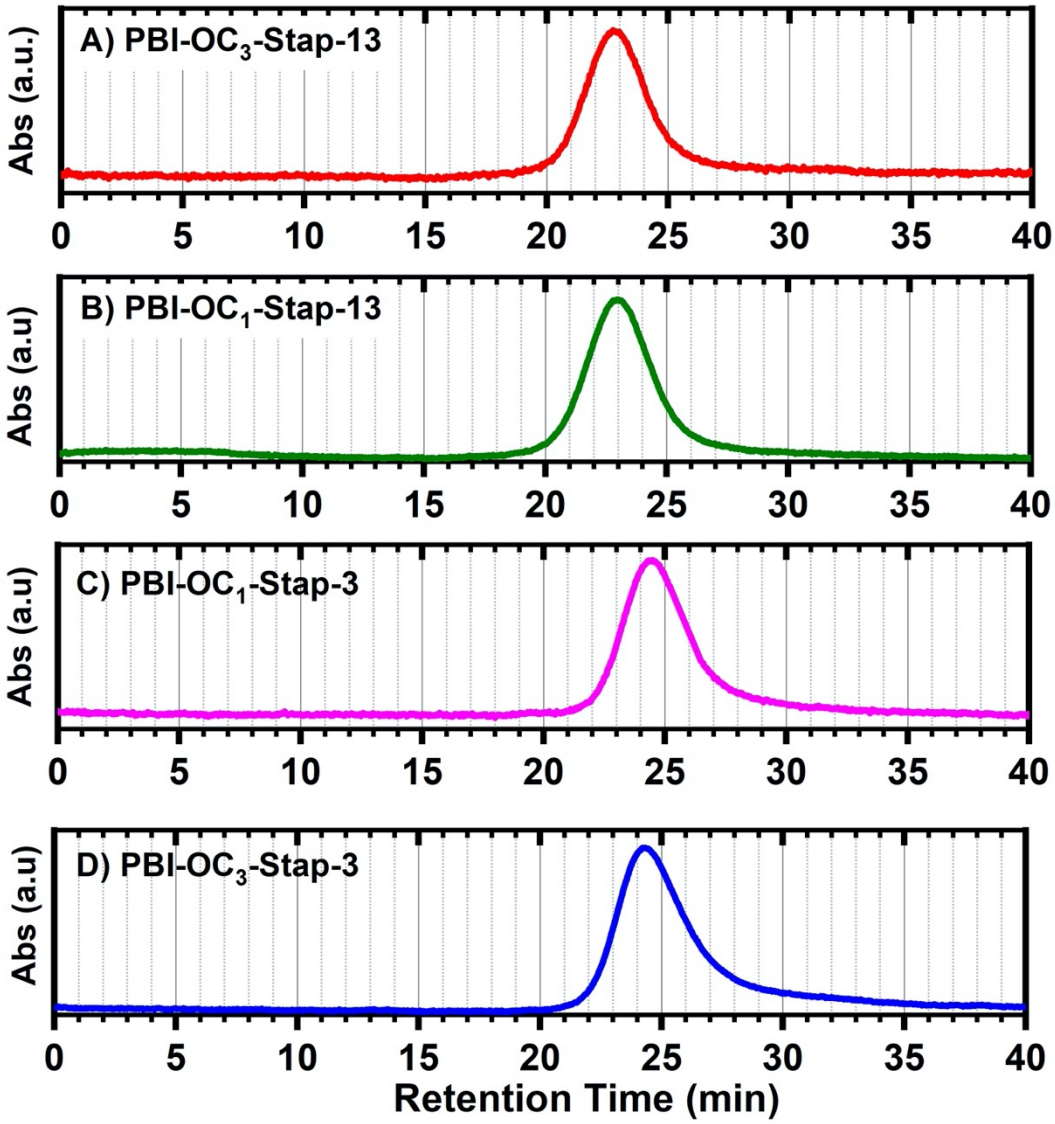

Figure S6. Elution time of the tethered assemblies recorded (A) **PBI-OC$_1$-Stap-3**; (B) **PBI-OC$_1$-Stap-13**; (C) **PBI-OC$_3$-Stap-3**; (D) **PBI-OC$_3$-Stap-13**. Sephacryl S-200 was used as the stationary phase and CH_3CN:H_2O 3:7 0.1M PBS as the mobile phase. The flow rate = 1 ml min^{-1}. $\lambda_{detection}$ = 490 nm.

Table S1. Weight Average Molecular Weight ($\bar{M}_w$) of Stapled PBI Assemblies and associated Poly Dispersity Index (PDI). The average numbers of repeating units have been calculated using $\bar{M}_w$ values.

Stapled Assemblies	$\bar{M}_w$ (g mol^{-1})	PDI	Repeating Units
PBI-OC$_1$-Stap-3	11,163	1.02	10
PBI-OC$_1$-Stap-13	18,300	1.03	12
PBI-OC$_3$-Stap-3	11,600	1.02	10
PBI-OC$_3$-Stap-13	19,350	1.03	12

The weight average molecular weight $\bar{M}_w$ values in Table S1 have been calculated based on the theoretical equation:

$$\bar{M} * = \frac{\sum_0^i N_i {M_i}^b}{\sum_0^i N_i {M_i}^{b-1}}$$

6. Microscopy Characterization

6.1 Scanning Electron Microscopy

Scanning electron microscope images were recorded with a Philips XL-30 Field Emission SEM (1 kV) at several magnifications. All samples were prepared by drop casting the solutions (20 μM) onto untreated silicon wafers.

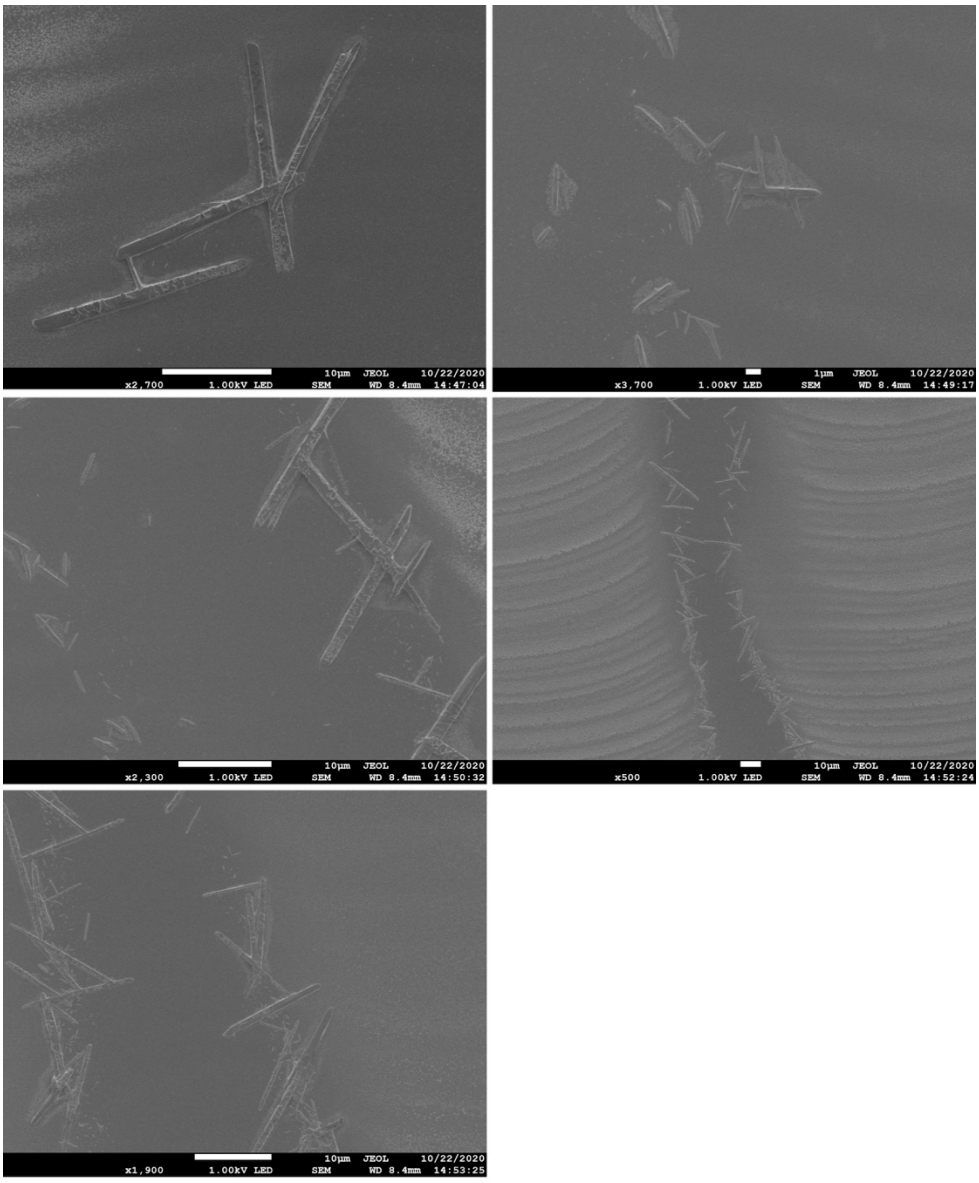

Figure S7. Scanning electron microscopy images of the non-covalent precursors **PBI-$OC_1C{\equiv}CH$** dropcast from a parent H_2O solution.

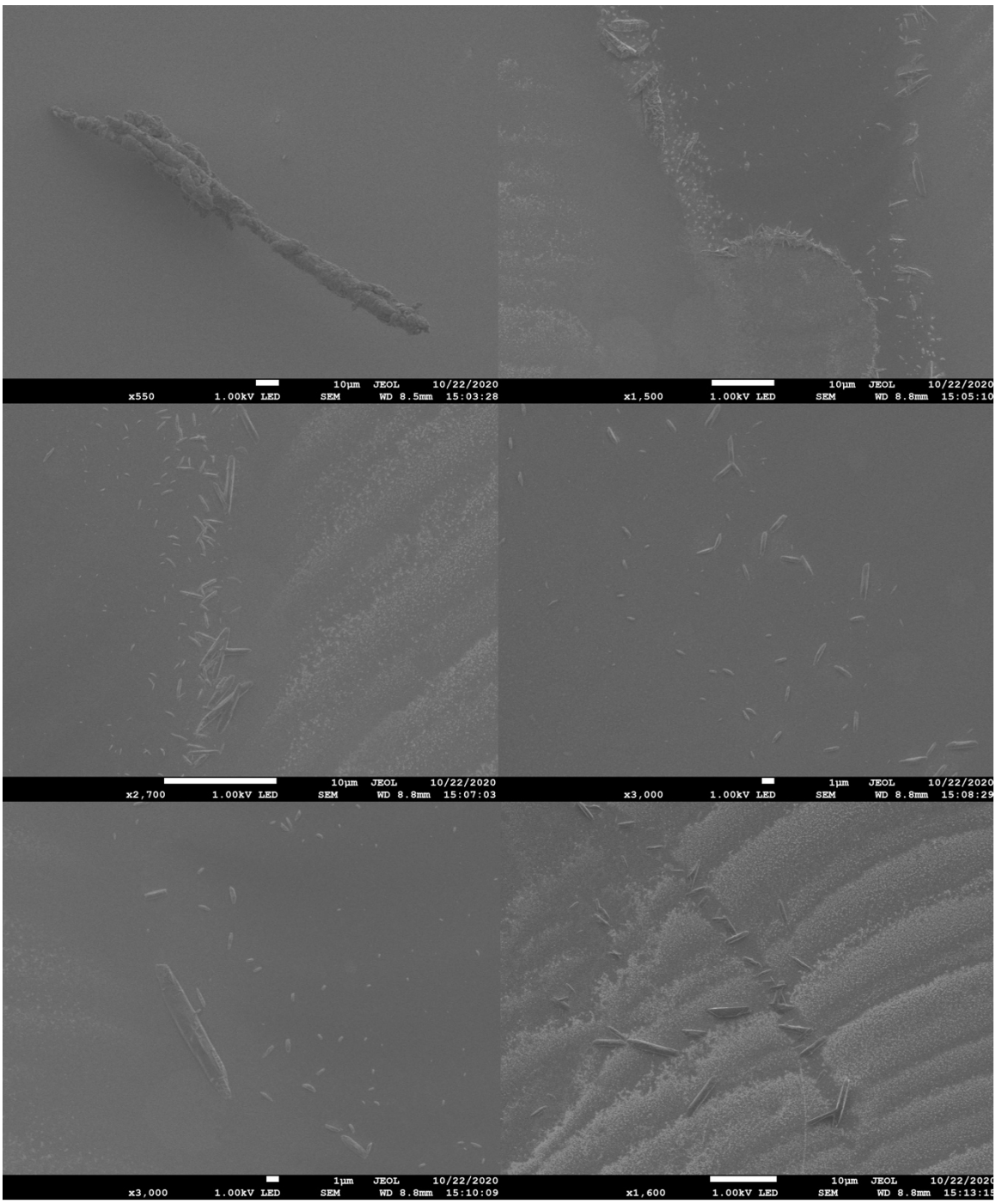

Figure S8. Scanning electron microscopy images of the non-covalent precursors **PBI-$OC_3C{\equiv}CH$** dropcast from a parent H_2O solution.

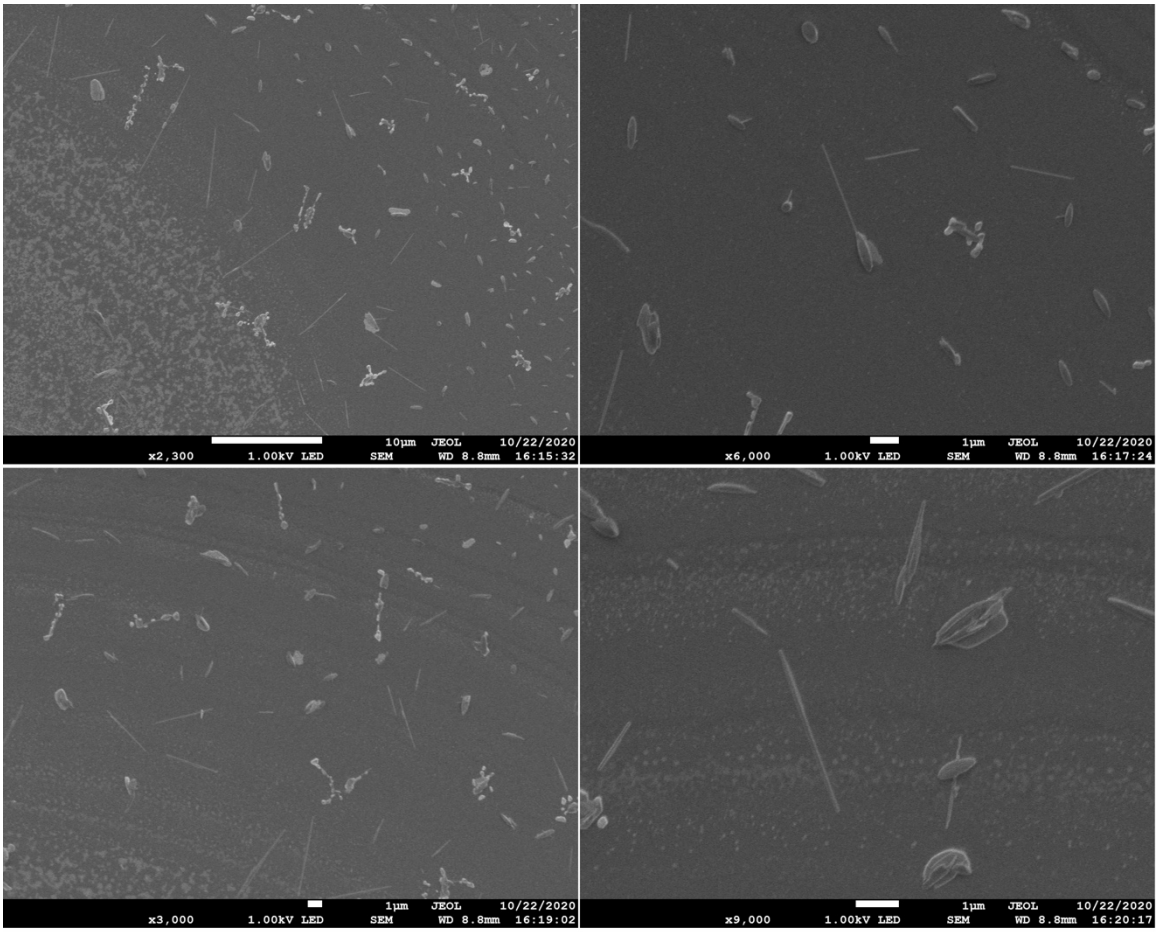

Figure S9. Scanning electron microscopy images of the stapled **PBI-OC$_1$-Stap-3** assemblies dropcast from a parent H_2O solution.

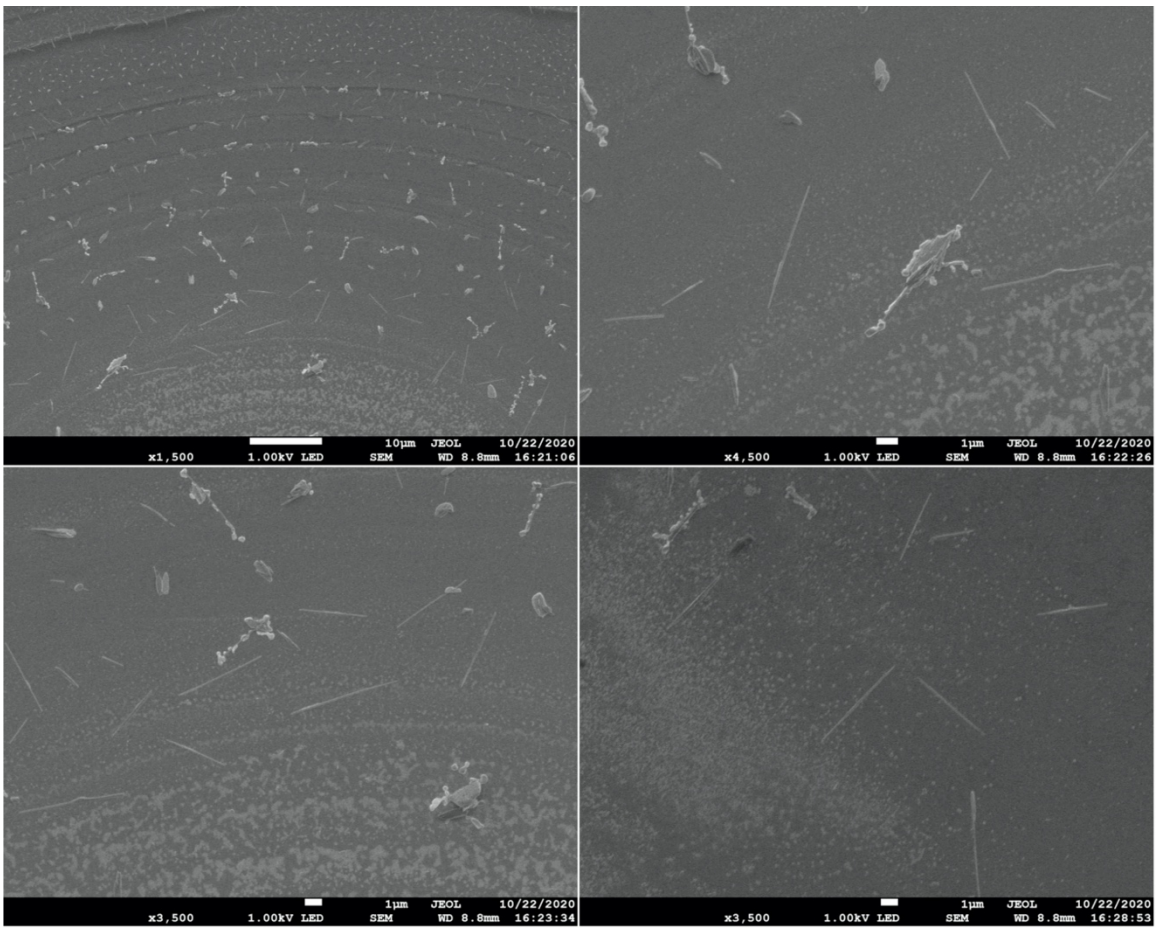

Figure S10. Scanning electron microscopy images of the stapled **PBI-OC$_1$-Stap-3** assembly dropcast from a parent H_2O solution.

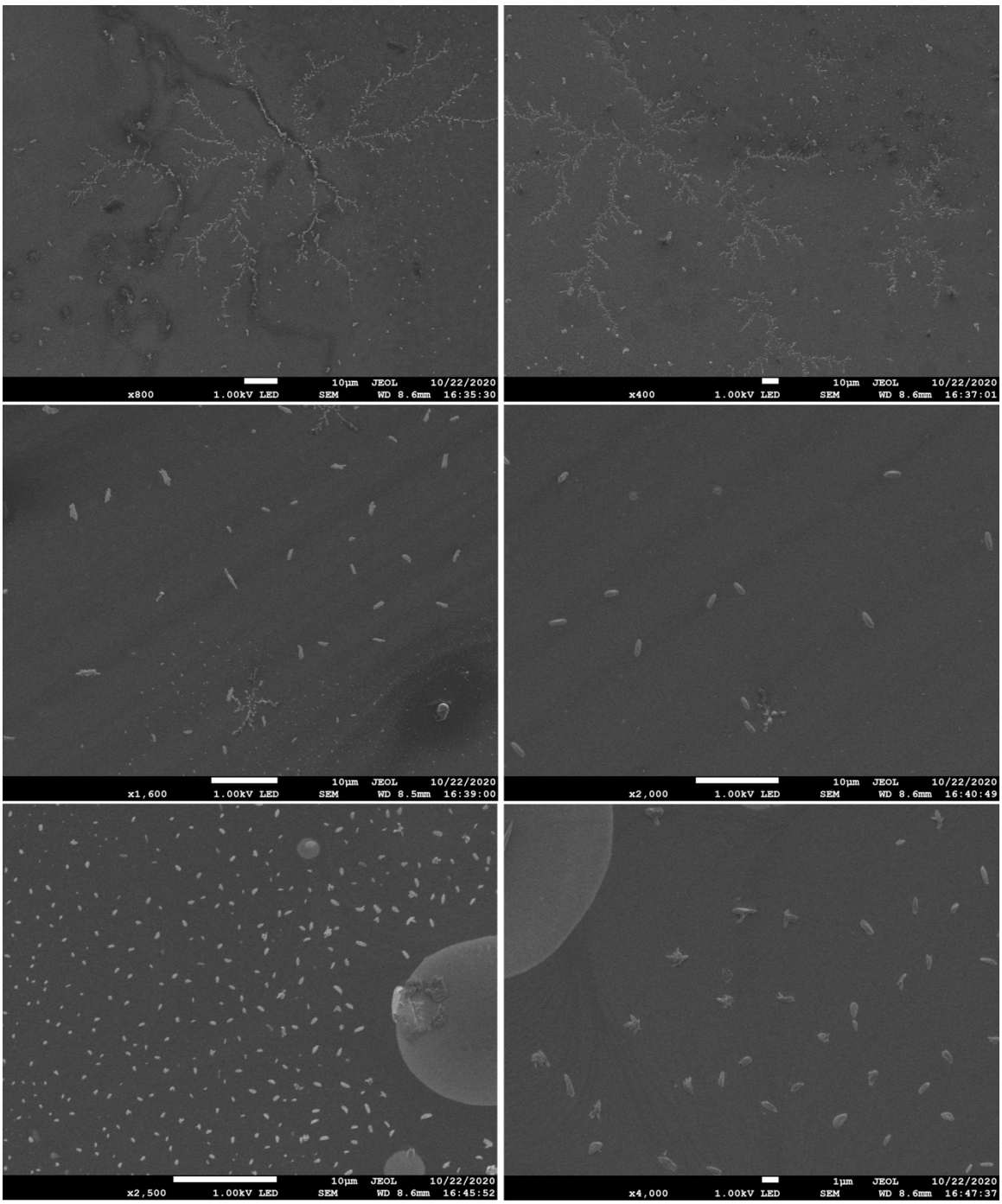

Figure S11. Scanning electron microscopy images of the stapled assemblies **PBI-OC$_1$-Stap-13** dropcast from a parent H_2O solution.

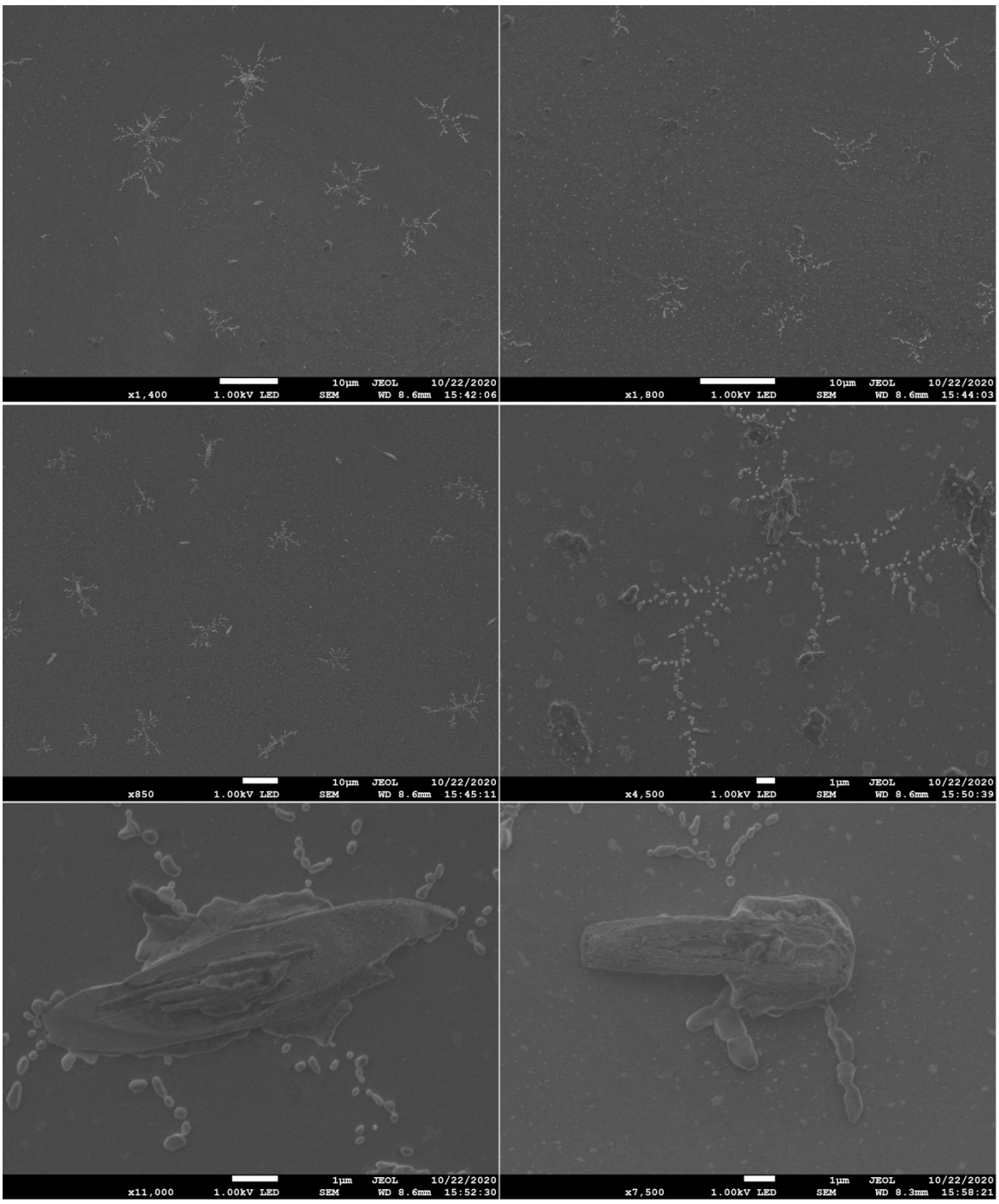

Figure S12. Scanning electron microscopy images of the stapled **PBI-OC$_3$-Stap-3** assemblies dropcast from a parent H_2O solution.

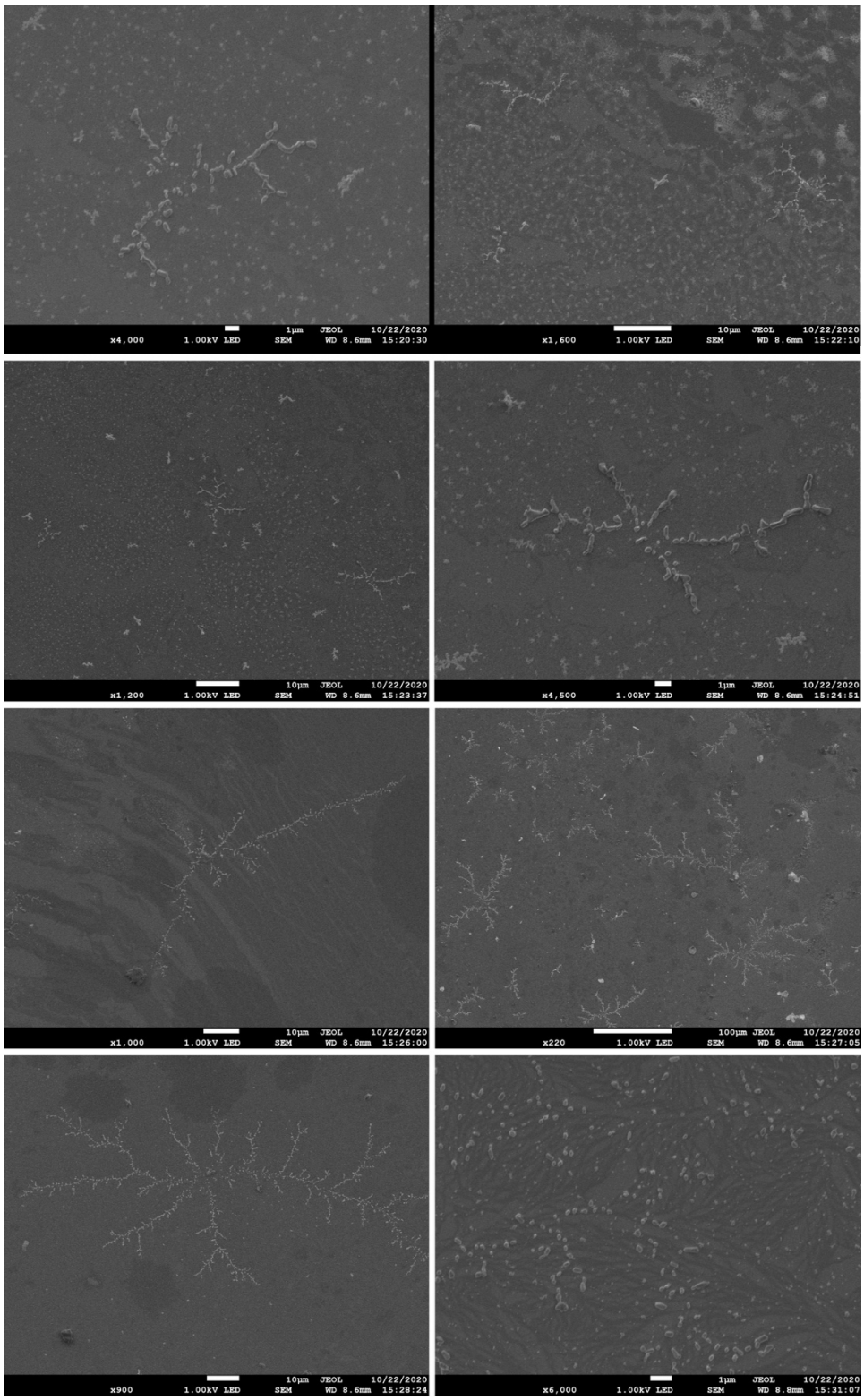

Figure S13. Scanning electron microscopy images of the stapled **PBI-OC$_3$-Stap-13** assemblies dropcast from a parent H_2O solution.

6.2 Atomic Force Microscopy

6.2.1 PBI-OC$_1$-Stap-3

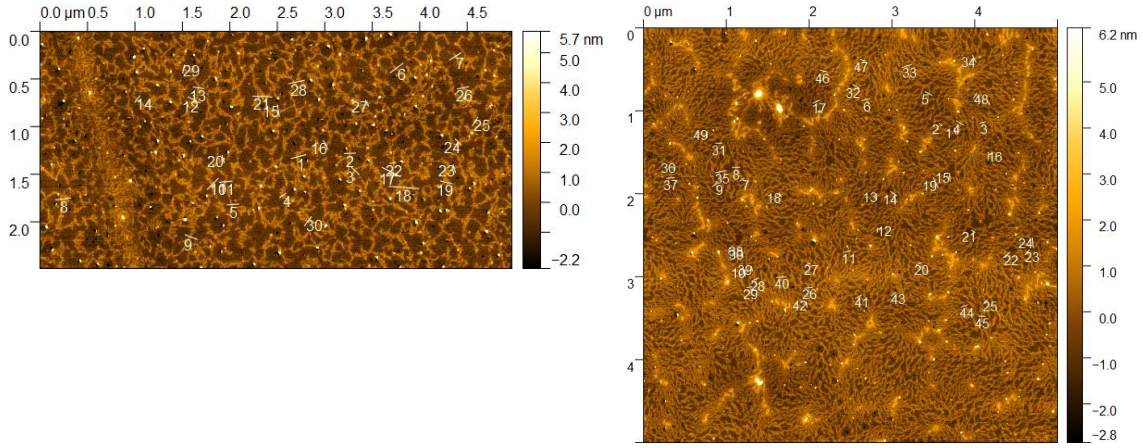

Figure S14. AFM images for the **PBI-OC$_1$-Stap-3** assembly drop cast from a parent water solution. The height profiles measured along the white lines are used to evaluate the thickness through the statistical analysis shown in Figure 3.

6.2.2 PBI-OC$_1$-Stap-13

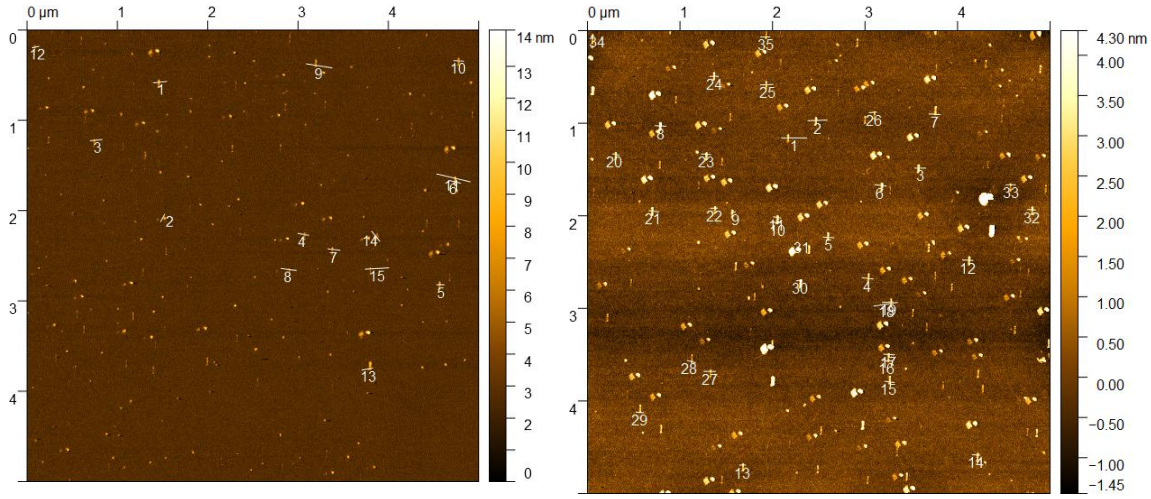

Figure S15. AFM images for the **PBI-OC$_1$-Stap-13** assembly drop cast from a parent water solution. The height profiles measured along the white lines are used to evaluate the thickness through the statistical analysis shown in Figure 3.

6.2.3 PBI-OC$_3$-Stap-3

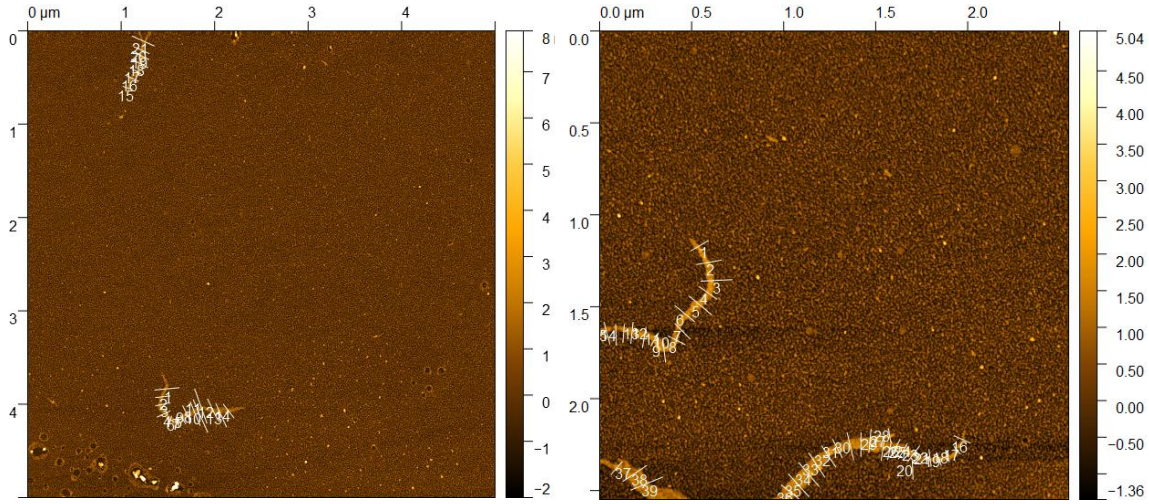

Figure S16. AFM images for the **PBI-OC$_3$-Stap-3** assembly drop cast from a parent water solution. The height profiles measured along the white lines are used to evaluate the thickness through the statistical analysis shown in Figure 3.

6.2.4 PBI-OC$_3$-Stap-13

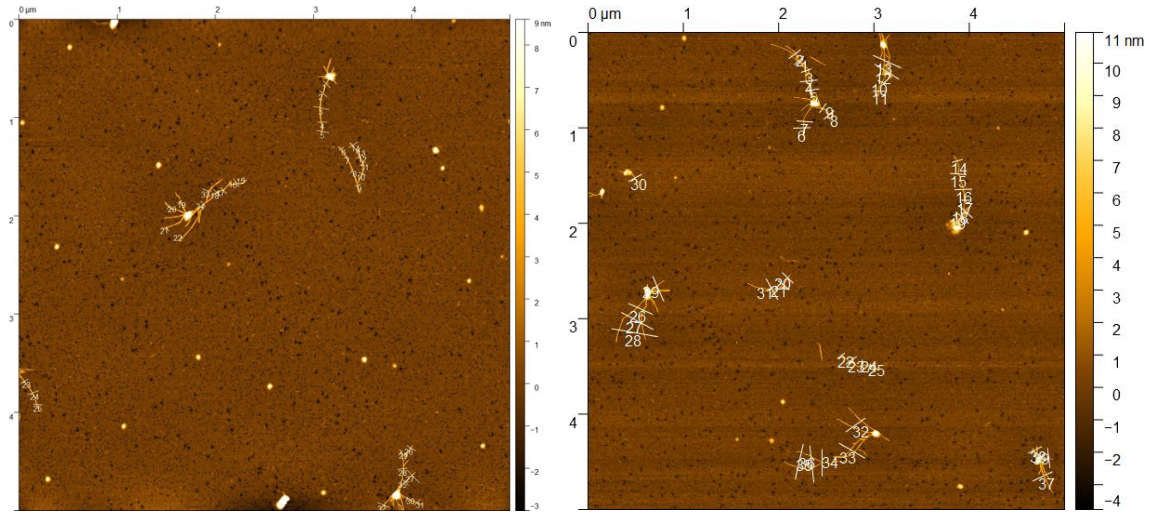

Figure S17. AFM images for the **PBI-OC$_3$-Stap-13** assembly drop cast from a parent water solution. The height profiles measured along the white lines are used to evaluate the thickness through the statistical analysis shown in Figure 3.

7. Solvent Dependence Spectroscopy of Bay-functionalized PBI monomers and Stapled Assemblies

Theoretical model developed for H-aggregates and adapted for PBI building blocks was utilized and is shown in equation S1.[6, 7] Please note that the Huang-Rhys factor has been calculated from Figure 4 ($\lambda^2 = 0.72$).

$$\frac{I_A^{0-0}}{I_A^{0-1}} \approx \left(\frac{1 - \frac{0.214W}{\hbar\omega_0}}{0.848\left(1 + \frac{0.164W}{\hbar\omega_0}\right)} \right)^2 \qquad \text{(eq. S8)}$$

Where I_A^{0-0} and I_A^{0-1} correspond to the oscillator strength of the first two vibronic transitions 0,0 and 0,1 respectively; W corresponds to the free-exciton bandwidth (Ex_{BW}); and $\hbar\omega_0$ is the energy associated to a symmetric ring-stretching mode (170 meV). Oscillator strengths of the 0-0 and 0-1 vibrionic transitions The results are presented in Table 2 in the main text as a function of the building blocks, the staplers, and the solvent. The corresponding deconvoluted spectra are shown below with the fitting parameters used. The excitonic coupling J_{12} has been calculated from the free-exciton bandwidth W=4 J_{12}.

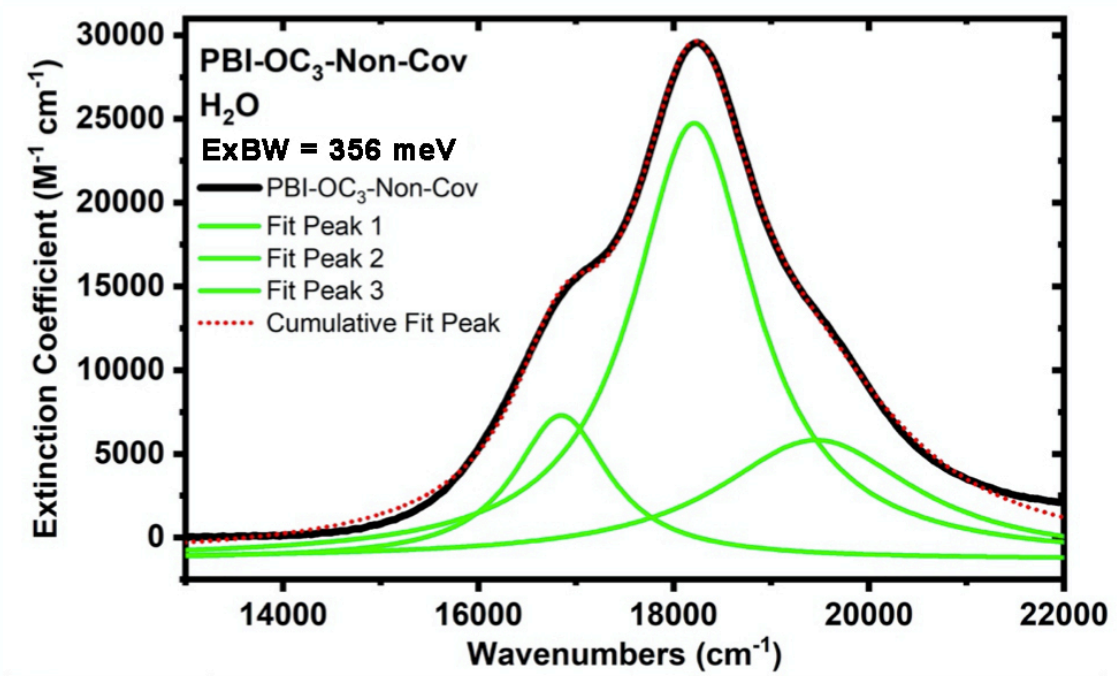

Model	Lorentz		
Equation	y = y0 + (2*A/pi)*(w/(4*(x-xc)^2 + w^2))		
Plot	Peak 1	Peak 2	Peak 3
y0	-1285.41007 ± 41.97119	-1285.41007 ± 41.97119	-1285.41007 ± 41.97119
xc	16849.29764 ± 10.01513	18212.38198 ± 5.97843	19460.59192 ± 56.69896
w	1186.50436 ± 32.49782	1530.62949 ± 32.72173	2477.11347 ± 98.66016
A	1.60169E7 ± 638645.05105	6.263E7 ± 2.3419E6	2.77114E7 ± 2.39603E6
Reduced Chi-Sqr	111316.80197		
R-Square (COD)	0.99857		
Adj. R-Square	0.99853		

Figure S18. Deconvolution of the experimental ground state electronic absorption spectra (black) recorded for the **PBI-OC$_3$-Non-Cov** assembly in H_2O at room temperature. The reconvoluted absorption spectrum is shown by the green lines. Peak 1, peak 2, and peak 3 correspond to the 0-0, 0-1, and 0-2 vibronic transitions, respectively. The extinction coefficient is provided per PBI units considering an initial PBI concentration of 20 μM in H_2O.

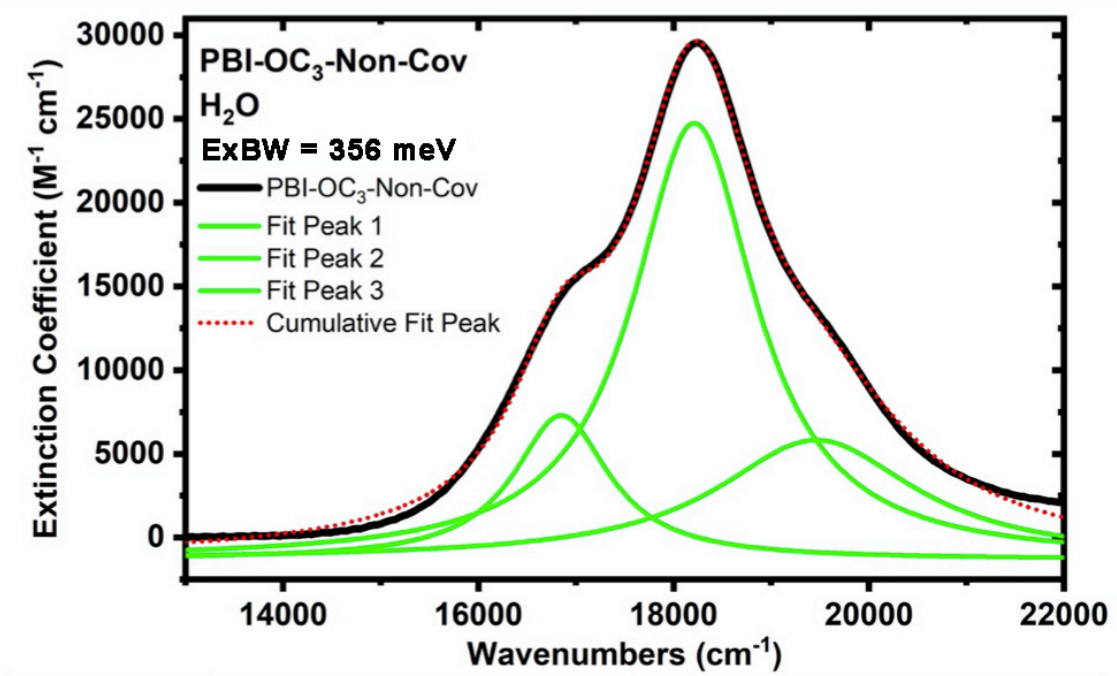

Model	Lorentz		
Equation	y = y0 + (2*A/pi)*(w/(4*(x-xc)^2 + w^2))		
Plot	Peak 1	Peak 2	Peak 3
y0	-1285.41007 ± 41.97119	-1285.41007 ± 41.97119	-1285.41007 ± 41.97119
xc	16849.29764 ± 10.01513	18212.38198 ± 5.97843	19460.59192 ± 56.69896
w	1186.50436 ± 32.49782	1530.62949 ± 32.72173	2477.11347 ± 98.66016
A	1.60169E7 ± 638645.05105	6.263E7 ± 2.3419E6	2.77114E7 ± 2.39603E6
Reduced Chi-Sqr	111316.80197		
R-Square (COD)	0.99857		
Adj. R-Square	0.99853		

Figure S19. Deconvolution of the experimental ground state electronic absorption spectra (black) recorded for the **PBI-OC$_1$-Non-Cov** assembly in H_2O at room temperature. The deconvoluted absorption spectra are shown by the green lines. Peak 1, peak 2, and peak 3 correspond to the 0-0, 0-1, and 0-2 vibronic transitions, respectively. The extinction coefficient is provided per PBI units considering an initial PBI concentration of 20 μM in H_2O.

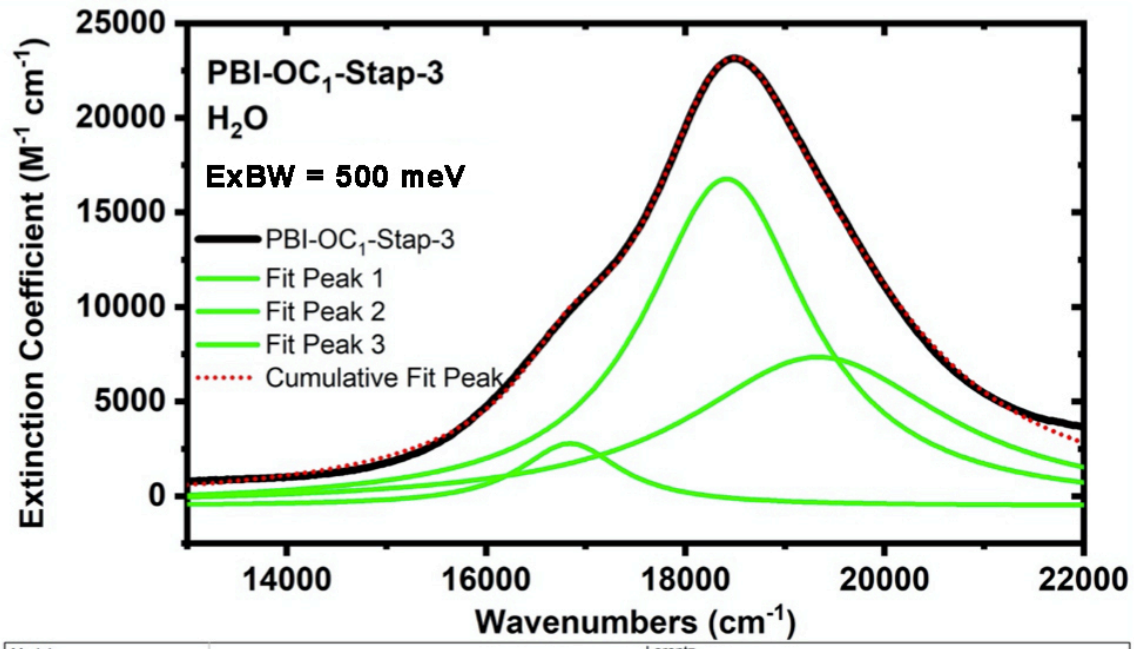

Model	Lorentz		
Equation	y = y0 + (2*A/pi)*(w/(4*(x-xc)^2 + w^2))		
Plot	Peak 1	Peak 2	Peak 3
y0	-507.37614 ± 51.05739	-507.37614 ± 51.05739	-507.37614 ± 51.05739
xc	19336.03554 ± 126.10008	18413.7444 ± 17.7548	16841.57416 ± 17.41814
w	3159.55568 ± 94.57289	1994.57332 ± 76.31025	1235.34341 ± 63.68251
A	3.90474E7 ± 6.97762E6	5.41357E7 ± 6.18114E6	6.40085E6 ± 526346.6209
Reduced Chi-Sqr	45758.9991		
R-Square (COD)	0.99907		
Adj. R-Square	0.99904		

Figure S20. Deconvolution of the experimental ground state electronic absorption spectra (black) recorded for the **PBI-OC$_1$-Stap-3** assembly in H_2O at room temperature. The deconvoluted absorption spectra are shown by the green lines. Peak 1, peak 2, and peak 3 correspond to the 0-0, 0-1, and 0-2 vibronic transitions, respectively. The extinction coefficient is provided per PBI units considering an initial PBI concentration of 20 μM.

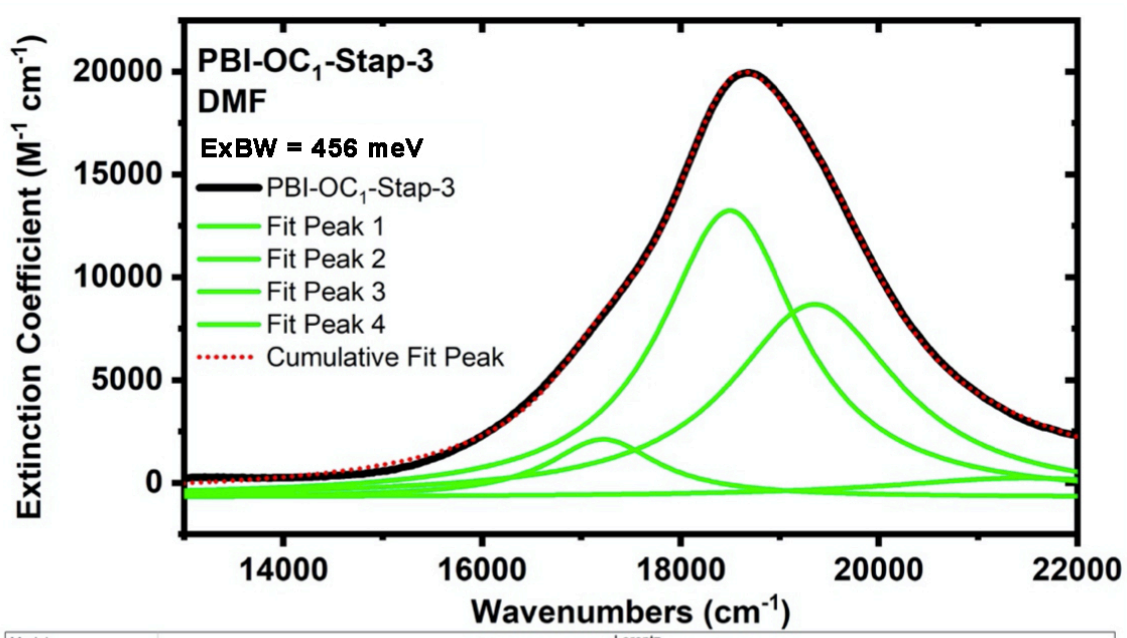

Model	Lorentz			
Equation	y = y0 + (2*A/pi)*(w/(4*(x-xc)^2 + w^2))			
Plot	Peak 1	Peak 2	Peak 3	Peak 4
y0	-691.32907 ± 30.23444	-691.32907 ± 30.23444	-691.32907 ± 30.23444	-691.32907 ± 30.23444
xc	17219.76082 ± 27.82374	18495.98844 ± 28.48969	19352.15042 ± 72.23329	21481.72322 ± 396.88875
w	1336.88722 ± 84.31325	1704.41833 ± 101.01746	2067.68855 ± 200.64093	3484.28432 ± 1919.93162
A	5.91195E6 ± 806876.81981	3.73107E7 ± 6.51029E6	3.04637E7 ± 8.40007E6	5.13595E6 ± 4.31597E6
Reduced Chi-Sqr	26694.00931			
R-Square (COD)	0.99931			
Adj. R-Square	0.99929			

Figure S21. Deconvolution of the experimental ground state electronic absorption spectra (black) recorded for the **PBI-OC$_1$-Stap-3** assembly in 90:10 DMF/H2O solvent mixture at room temperature. The deconvoluted absorption spectra are shown by the green lines. Peak 1, peak 2, and peak 3 correspond to the 0-0, 0-1, and 0-2 vibronic transitions, respectively. The extinction coefficient is provided per PBI units considering an initial PBI concentration of 20 μM.

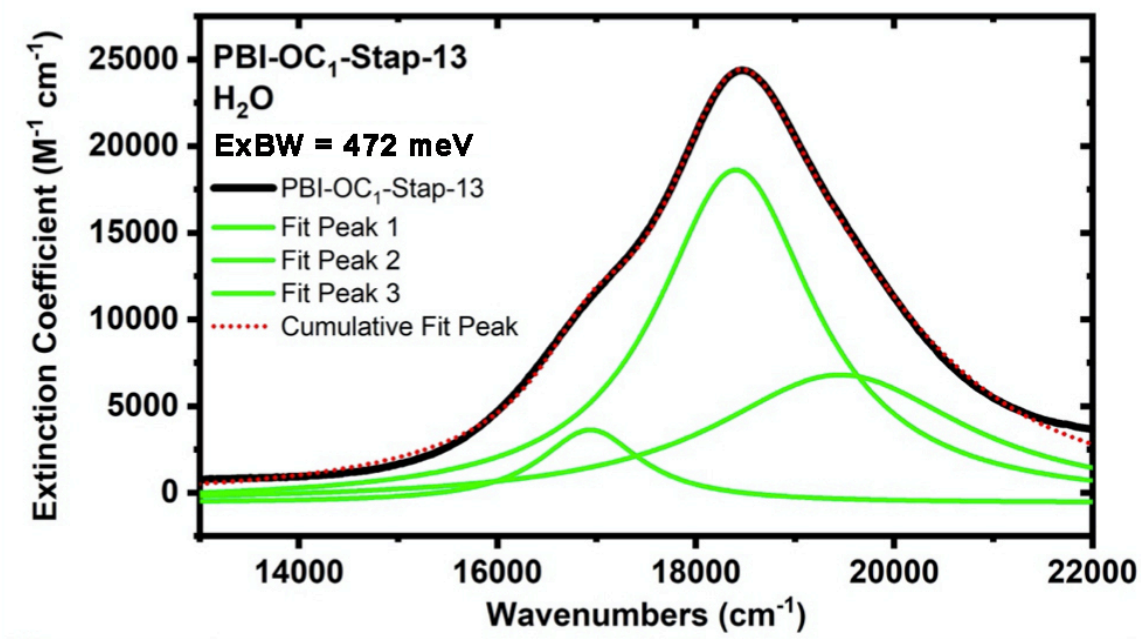

Model	Lorentz		
Equation	y = y0 + (2*A/pi)*(w/(4*(x-xc)^2 + w^2))		
Plot	Peak 1	Peak 2	Peak 3
y0	-578.01857 ± 50.1636	-578.01857 ± 50.1636	-578.01857 ± 50.1636
xc	169375.1748 ± 172.73632	184054.53633 ± 140.62666	194552.88422 ± 1195.009
w	12444.76655 ± 596.81706	19289.43636 ± 694.3344	31297.69324 ± 1160.76786
A	8.24213E7 ± 6.61648E6	5.81886E8 ± 5.28542E7	3.63184E8 ± 5.86219E7
Reduced Chi-Sqr	60886.92163		
R-Square (COD)	0.99888		
Adj. R-Square	0.99885		

Figure S22. Deconvolution of the experimental ground state electronic absorption spectra (black) recorded for the **PBI-OC$_1$-Stap-13** assembly in H_2O at room temperature. The deconvoluted absorption spectra are shown by the green lines. Peak 1, peak 2, and peak 3 correspond to the 0-0, 0-1, and 0-2 vibronic transitions, respectively. The extinction coefficient is provided per PBI units considering an initial PBI concentration of 20 μM.

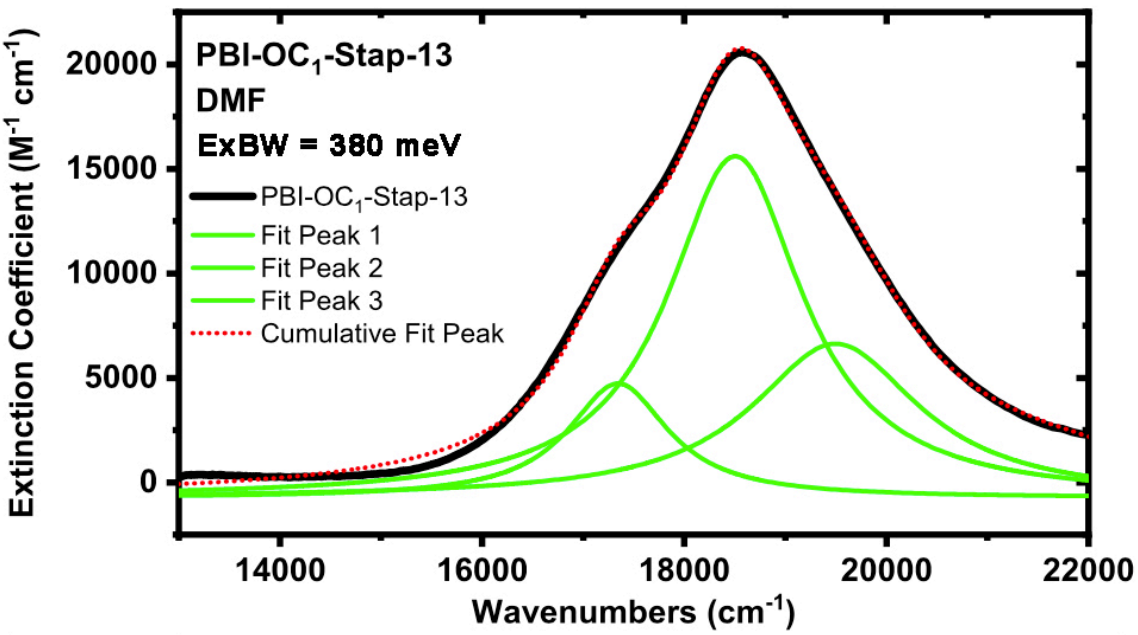

Model	Lorentz			
Equation	y = y0 + (2*A/pi)*(w/(4*(x-xc)^2 + w^2))			
Plot	Peak 1	Peak 2	Peak 3	Peak 4
y0	-738.88449 ± 39.11402	-738.88449 ± 39.11402	-738.88449 ± 39.11402	-738.88449 ± 39.11402
xc	17344.12064 ± 22.09501	18504.08377 ± 23.34021	19495.88801 ± 90.45306	21571.91811 ± 374.01048
w	1205.45748 ± 69.93864	1622.80588 ± 113.26726	2016.5411 ± 319.69547	3014.83885 ± 2133.39503
A	1.03586E7 ± 1.27848E6	4.16554E7 ± 6.76861E6	2.33412E7 ± 8.67683E6	5.00106E6 ± 5.04986E6
Reduced Chi-Sqr	78448.73371			
R-Square (COD)	0.99812			
Adj. R-Square	0.99806			

Figure S23. Deconvolution of the experimental ground state electronic absorption spectra (black) recorded for the **PBI-OC$_1$-Stap-13** assembly in a 90:10 DMF/H_2O solvent mixture at room temperature. The deconvoluted absorption spectra are shown by the green lines. Peak 1, peak 2, and peak 3 correspond to the 0-0, 0-1, and 0-2 vibronic transitions, respectively. The extinction coefficient is provided per PBI units considering an initial PBI concentration of 20 μM.

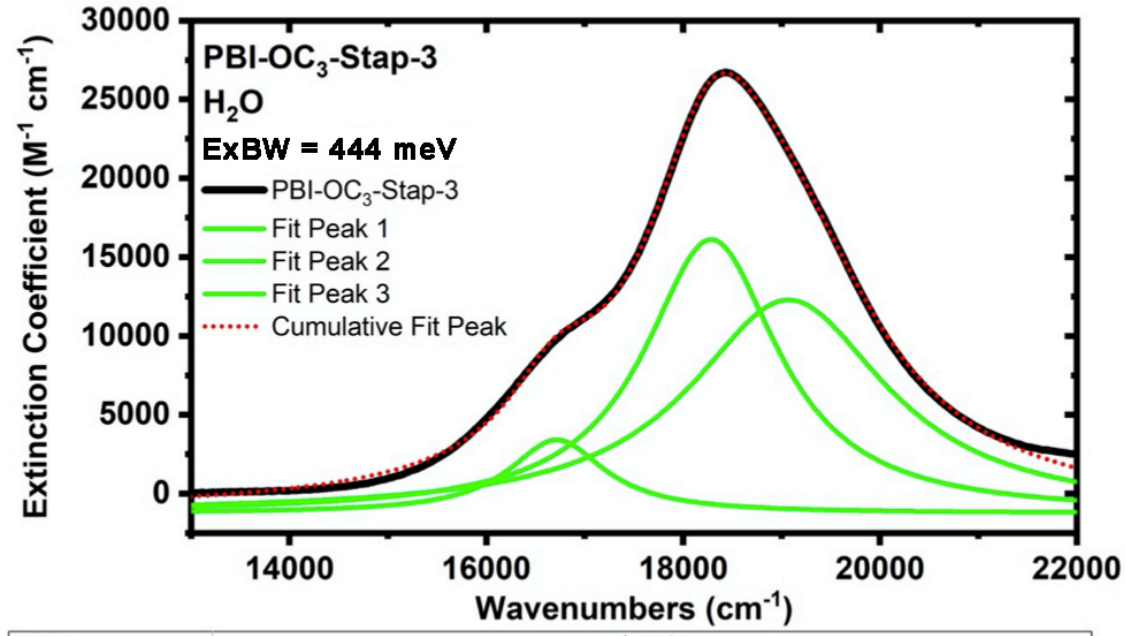

Model	Lorentz		
Equation	y = y0 + (2*A/pi)*(w/(4*(x-xc)^2 + w^2))		
Plot	Peak 1	Peak 2	Peak 3
y0	-1218.30689 ± 38.72747	-1218.30689 ± 38.72747	-1218.30689 ± 38.72747
xc	16714.51181 ± 12.40681	18284.62475 ± 18.34668	19069.71584 ± 56.74451
w	1181.29297 ± 42.65662	1656.15573 ± 62.39515	2427.18574 ± 44.06888
A	8.62042E6 ± 430996.44798	4.51139E7 ± 5.06779E6	5.15358E7 ± 5.42278E6
Reduced Chi-Sqr	61959.5969		
R-Square (COD)	0.99909		
Adj. R-Square	0.99906		

Figure S24. Deconvolution of the experimental ground state electronic absorption spectra (black) recorded for the **PBI-OC$_1$-Stap-13** assembly in H_2O at room temperature. The deconvoluted absorption spectra are shown by the green lines. Peak 1, peak 2, and peak 3 correspond to the 0-0, 0-1, and 0-2 vibronic transitions, respectively. The extinction coefficient is provided per PBI units considering an initial PBI concentration of 20 μM.

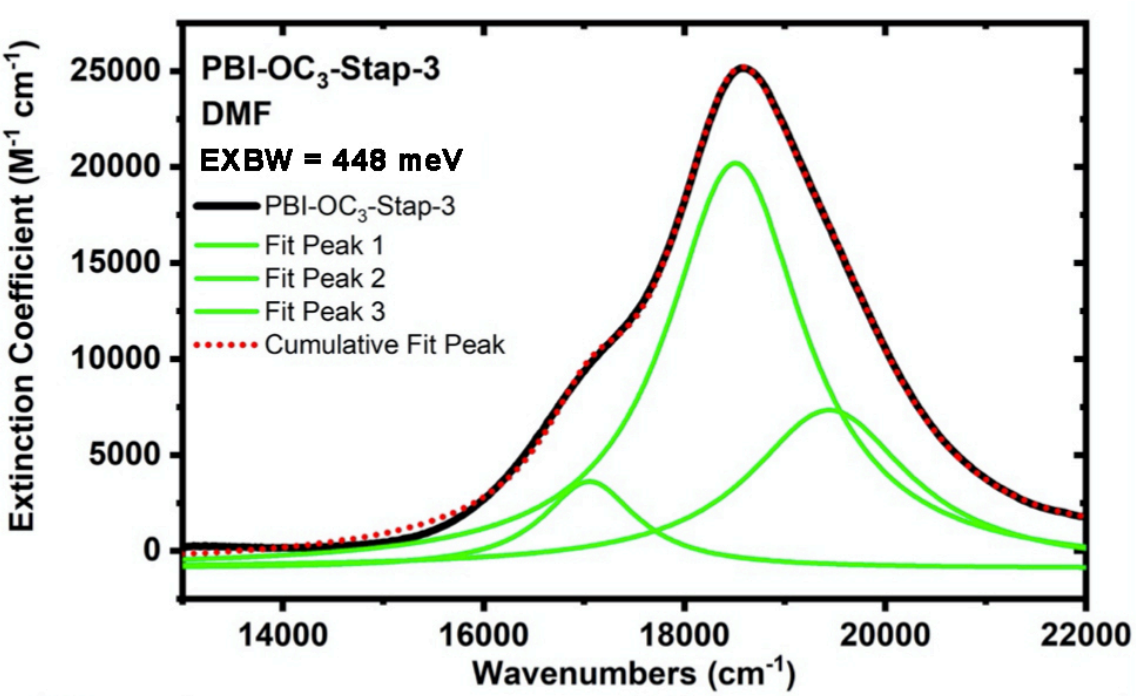

Model	Lorentz			
Equation	y = y0 + (2*A/pi)*(w/(4*(x-xc)^2 + w^2))			
Plot	Peak 1	Peak 2	Peak 3	Peak 4
y0	-903.67107 ± 29.24375	-903.67107 ± 29.24375	-903.67107 ± 29.24375	-903.67107 ± 29.24375
xc	17054.55299 ± 15.03967	18508.17911 ± 16.14749	19443.13306 ± 59.83599	22476.89679 ± 1611.4968
w	1140.92545 ± 54.30567	1660.82801 ± 54.30114	1938.34345 ± 124.95605	1492.89854 ± 1499.11173
A	8.11632E6 ± 608388.86363	5.50664E7 ± 4.26532E6	2.51165E7 ± 4.38451E6	1.54641E6 ± 3.62567E6
Reduced Chi-Sqr	70552.66447			
R-Square (COD)	0.99878			
Adj. R-Square	0.99873			

Figure S25. Deconvolution of the experimental ground state electronic absorption spectra (black) recorded for the **PBI-OC$_3$-Stap-3** assembly in a 90:10 DMF/H2O solvent mixture at room temperature. The deconvoluted absorption spectra are shown by the green lines. Peak 1, peak 2, and peak 3 correspond to the 0-0, 0-1, and 0-2 vibronic transitions, respectively. The extinction coefficient is provided per PBI units considering an initial PBI concentration of 20 μM.

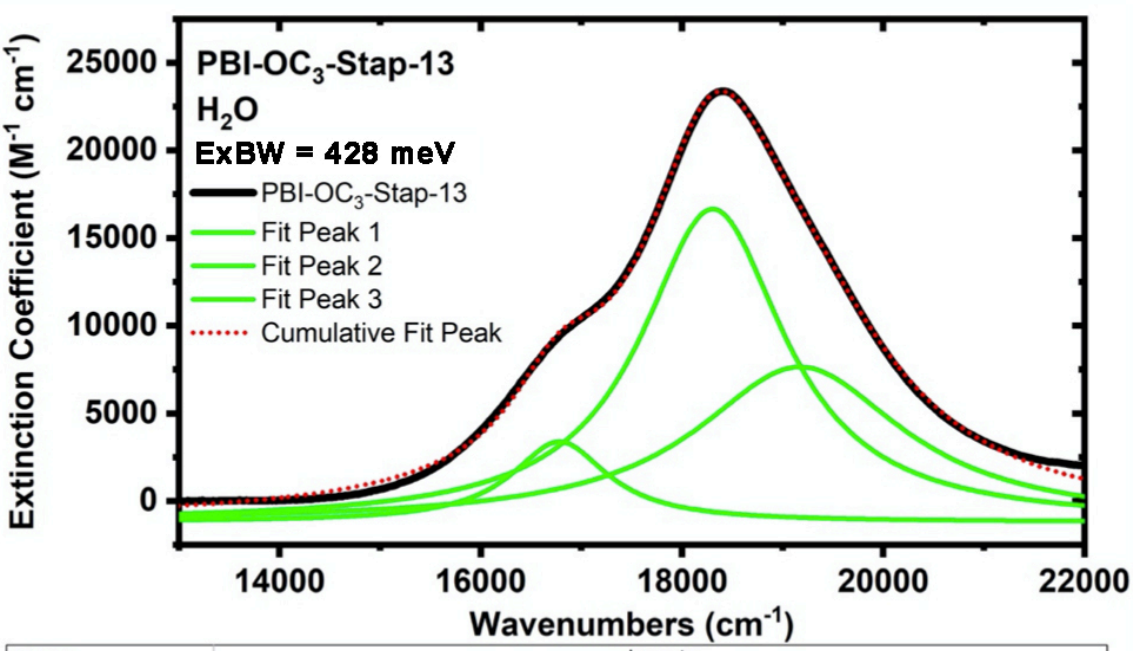

Model	Lorentz		
Equation	y = y0 + (2*A/pi)*(w/(4*(x-xc)^2 + w^2))		
Plot	Peak 1	Peak 2	Peak 3
y0	-1180.09662 ± 38.36477	-1180.09662 ± 38.36477	-1180.09662 ± 38.36477
xc	16782.01259 ± 13.49959	18306.03148 ± 18.00862	19171.09468 ± 83.37597
w	1158.65645 ± 47.29965	1733.08711 ± 65.03273	2504.62491 ± 72.79947
A	8.32387E6 ± 500841.82937	4.85584E7 ± 4.99201E6	3.4771E7 ± 5.20426E6
Reduced Chi-Sqr	65790.52756		
R-Square (COD)	0.99873		
Adj. R-Square	0.9987		

Figure S26. Deconvolution of the experimental ground state electronic absorption spectra (black) recorded for the **PBI-OC$_3$-Stap-13** assembly in H_2O at room temperature. The deconvoluted absorption spectra are shown by the green lines. Peak 1, peak 2, and peak 3 correspond to the 0-0, 0-1, and 0-2 vibronic transitions, respectively. The extinction coefficient is provided per PBI units considering an initial PBI concentration of 20 μM.

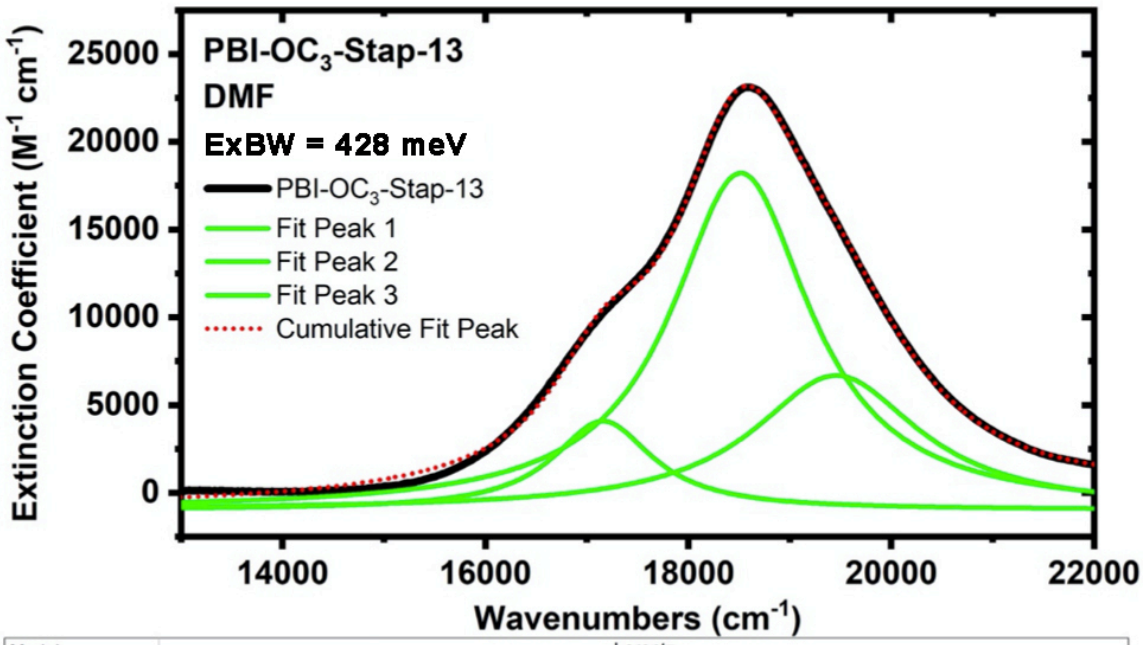

Model	Lorentz			
Equation	y = y0 + (2*A/pi)*(w/(4*(x-xc)^2 + w^2))			
Plot	Peak 1	Peak 2	Peak 3	Peak 4
y0	-953.3829 ± 29.67166	-953.3829 ± 29.67166	-953.3829 ± 29.67166	-953.3829 ± 29.67166
xc	17158.26371 ± 15.80498	18517.52273 ± 18.24629	19456.84875 ± 71.53112	22464.10621 ± 1872.91495
w	1187.5337 ± 54.45239	1660.72838 ± 68.1137	1981.47775 ± 158.59687	1887.02721 ± 2543.35755
A	9.41832E6 ± 758206.80634	5.0028E7 ± 4.86255E6	2.38062E7 ± 5.11335E6	1.74057E6 ± 4.25799E6
Reduced Chi-Sqr	66534.90264			
R-Square (COD)	0.99868			
Adj. R-Square	0.99863			

Figure S27. Deconvolution of the experimental ground state electronic absorption spectra (black) recorded for the **PBI-OC$_3$-Stap-13** assembly in a 90:10 DMF/H2O solvent mixture at room temperature. The deconvoluted absorption spectra are shown by the green lines. Peak 1, peak 2, and peak 3 correspond to the 0-0, 0-1, and 0-2 vibronic transitions, respectively. The extinction coefficient is provided per PBI units considering an initial PBI concentration of 20 μM.

8. Steady-State Fluorescence Spectroscopy Experiments

All samples were prepared by diluting stock solutions of **PBI-OC$_3$C≡CH**, **PBI-OC$_1$C≡CH**, **PBI-OC$_1$-Stap-3**, **PBI-OC$_1$-Stap-13**, **PBI-OC$_3$-Stap-3**, and **PBI-OC$_3$-Stap-13** to 1 μM in H_2O and DMF. For the stapled samples, the concentration was approximated by matching the optical densities of tethered superstructures to that of unstapled analytes, which are known. Consequently, the reported concentration corresponds to that of PBI repeating units.

Each measurement was taken in a 4 mm pathlength quartz cuvette. The wavelength of excitation, 545 nm, corresponds to the 0-1 transition of the S1 state of -O bay-functionalized PBI. This wavelength was chosen as it features the maximum absorbance of PBI in the aggregated form. Refer to Figure 2. Emission spectra were normalized using the maximum fluorescence intensity of untethered PBI monomers **PBI-OC$_3$C≡CH** and **PBI-OC$_1$C≡CH** as the highest normalized value (y = 1) The emission range was set from 560 to 900 nm with a bandwidth of excitation/emission of 5 nm. All experiments were repeated 3 times to ensure reproducibility. Rhodamine B (1 μM, Φ_F = 0.31 in H_2O)[8] was used as an internal reference to determine the fluorescence quantum yields (Φ_F) of the PBI derivatives.

The Φ_F values were calculated using the equation:[9]

$$\Phi_s = \Phi_r \left(\frac{A_r}{A_s}\right)\left(\frac{I_s}{I_r}\right)\left(\frac{n_S}{n_r}\right)^2$$

Where Φ_s is the fluorescence quantum yield of the unknown sample, Φ_r is the fluorescence quantum yield of the reference, A_r and A_s are the integrated absorbances of the reference and unknown samples, I_s and I_r are the integrated fluorescence intensities of reference and unknown samples, n_s and n_r correspond to the refractive indexes of the reference and unknown samples, respectively. The integrated areas for absorption and fluorescence were calculated using an absolute integral function in OriginPro 2018 by selecting the area under the curve from 450 to 700 nm for absorption and 560 to 800 for emission spectra. The refractive index values utilized were 1.333 for H_2O and 1.4305 for DMF. All reported quantum yield calculations were twice reproduced from freshly made sample batches.

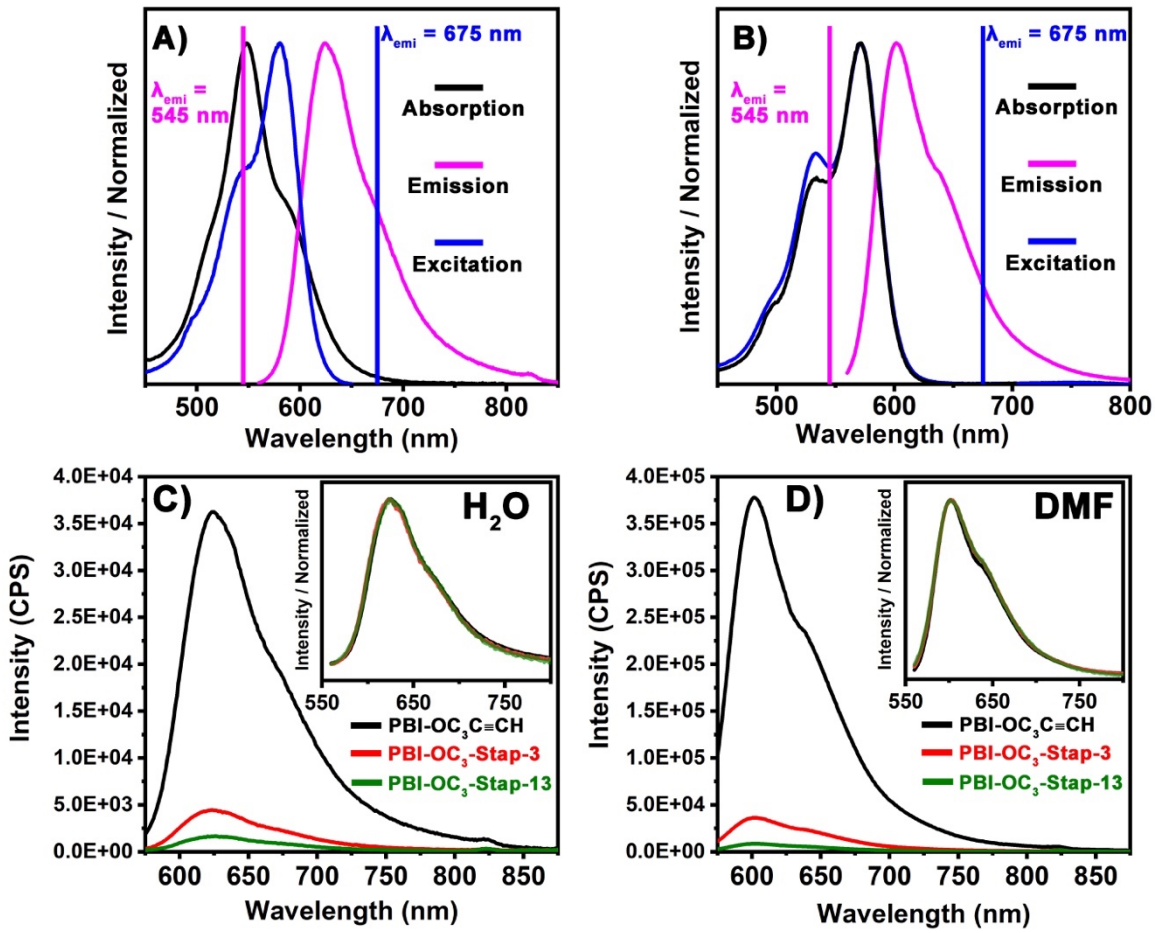

Figure S28. Normalized emission (λ_{exc} = 545 nm) and excitation spectra (λ_{emi} = 625 nm) of the precursor building block **PBI-OC$_3$C≡CH** solvated in water (A) and DMF (B). The normalized absorption spectra are shown as visual aids. (C-D) Steady-state photoluminescence spectra (λ_{exc} = 545 nm) of the stapled assemblies **PBI-OC$_3$-Stap-1/13** are compared to that of the parent non-covalent precursors **PBI-OC$_3$C≡CH** in water (C) and DMF (D). The concentration of the three samples is kept identical at 1 μM of PBI building blocks.

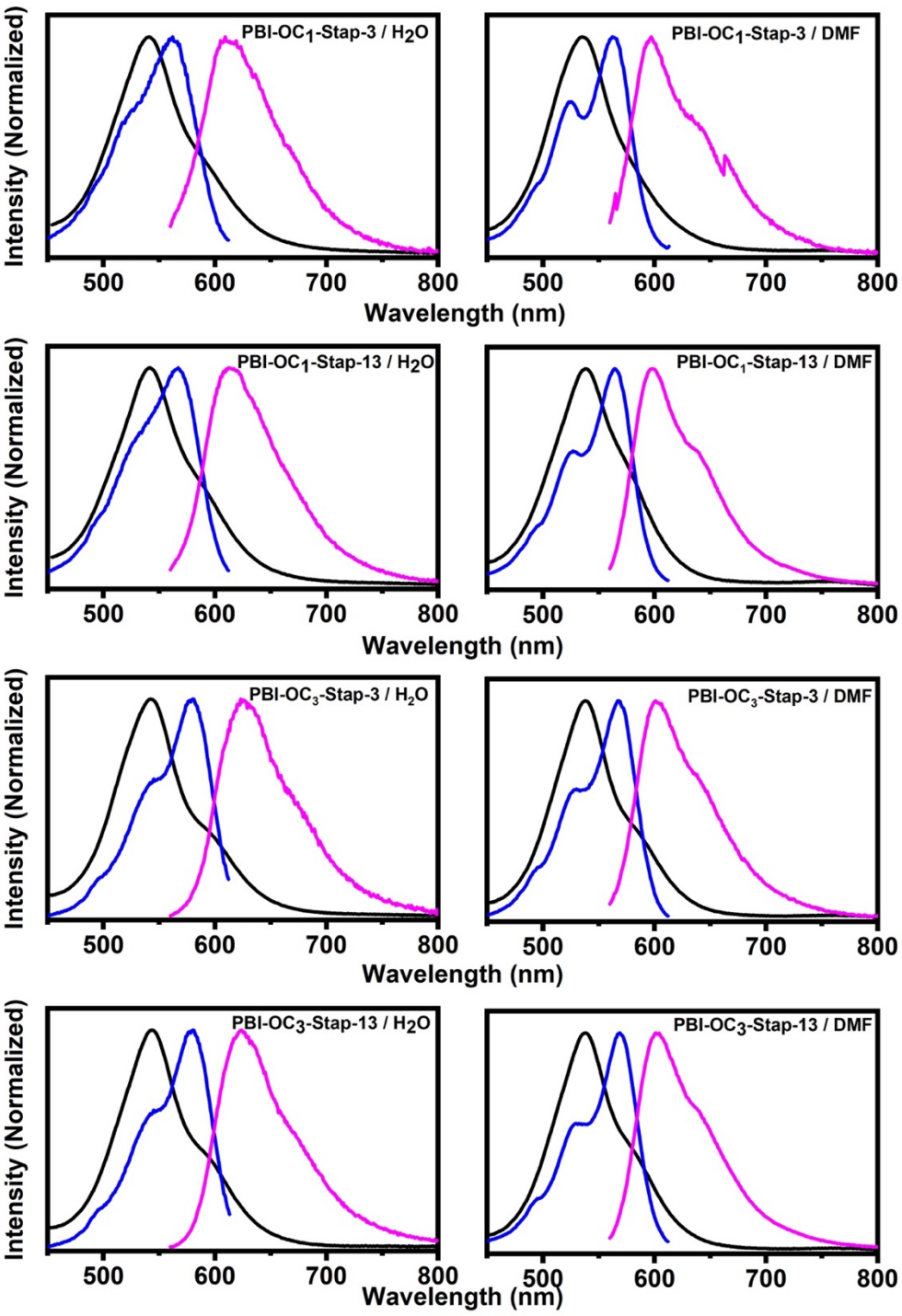

Figure S29. Emission (purple line, λ_{exc} = 545 nm) and excitation spectra (blue line, λ_{exc} = 625 nm) recorded for the stapled assemblies in H_2O and DMF solvents. Experimental conditions: [PBI] = 1 μm, room temperature, optical path length = 4 mm. Please note that the concentration of [PBI] is per repeating unit. For comparison, the normalized absorption spectra are overlaid (black line).

9. DFT and TD-DFT Calculations (p. 32-34)

Structure optimization calculations were performed using density functional theory (DFT) in the Gaussian 09.D01 software package. For the tetramer aggregate model, the calculations were conducted using the truncated molecular structure shown in Figure S24 where the pendant ammonium side chains connected on the imide positions have been replaced by a methyl fragment. To account for dispersion forces, the ωB97X-D functional from Head-Gordon and coworkers was exploited. Furthermore, the Dunning's correlation consistent double zeta basis set (cc-pvdz) was utilized. The energy-minimized tetramer was obtained by iterative minimization of a dimer and a trimer model aggregate. The xyz coordinates are attached.

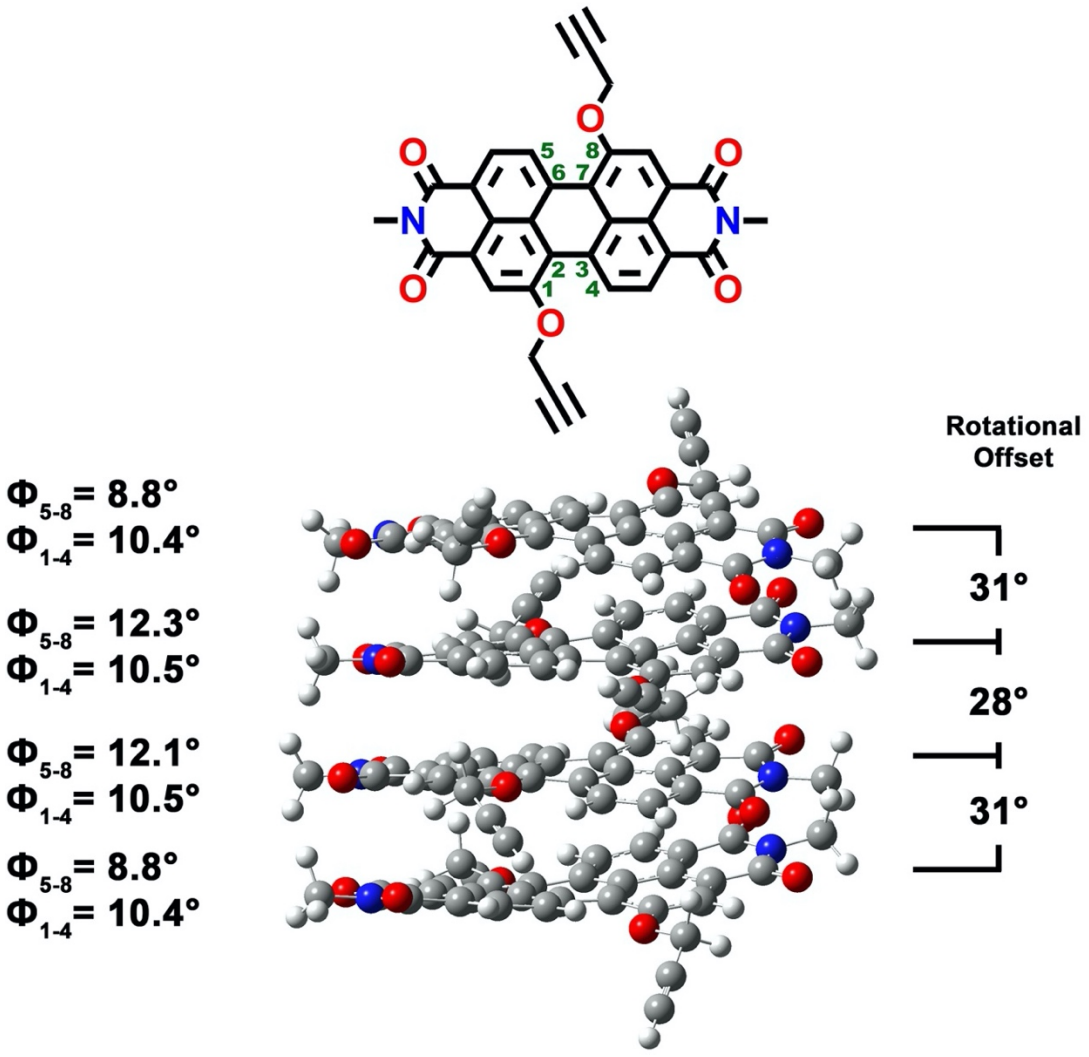

Figure S30: Energy-minimized structure of a model PBI tetramer aggregate built from the building block shown at the top. The pendant ammonium side chains have been truncated to methyl fragments. The alkoxy side chains flanked on the PBI bay regions contort the aromatic cores. The dihedral angles are provided on the left while the rotational offset between each PBI unit is shown on the right.

XYZ coordinate:

C -3.4286199961 -0.3068499999 2.8224299989
C -3.9904799985 -1.0068500011 1.7819499977
C -3.4832699997 -0.8291799970 0.4793599997
C -2.4165799996 0.0715400002 0.2135500001
C -1.7866899967 0.7215799980 1.3286299982
C -2.3280400006 0.5259299997 2.5980300012
H -3.8752699974 -0.3929199997 3.8192400001
C -4.0725699994 -1.5544399991 -0.5743599988
C -2.0138400013 0.3151400001 -1.1409499987
H -1.8940899984 1.0394500001 3.4453700000
C -2.6184799962 -0.4513199996 -2.1562800010
C -3.6276099996 -1.3844499968 -1.8573400013
H -4.1081099958 -1.9578499993 -2.6576999968
C -5.1731899954 -2.5182299988 -0.3246799999
C -5.1515399958 -1.8901499989 2.0477699972
N -5.6570299834 -2.6128100000 0.9676099976
C -6.7596400191 -3.5412099986 1.1911700006
H -6.4403800009 -4.5550999986 0.9183100021
H -7.0176800024 -3.4954700004 2.2519699990
H -7.6189799895 -3.2389999959 0.5797000001
O -5.6500899831 -3.1965499982 -1.2214100015
O -5.6473600108 -1.9770300008 3.1562799990
C -1.0174099969 1.3754200005 -1.3821199978
C -0.6280399994 1.6008300016 1.0896799981
C -0.3262999997 1.9565800005 -0.2641800000
C -0.7365199989 1.8638599990 -2.6557099994
H -1.2646800016 1.4601700005 -3.5083999956
C 0.6886000022 2.9153999996 -0.5293200015
C 0.9346099989 3.3837999990 -1.8368399990
C 0.1914000000 2.1269600012 2.1085200011
C 1.2323499994 3.0228399965 1.8117199993
H 1.8531099968 3.4370599969 2.6130700007
C 0.2036899999 2.8742299969 -2.8813799959
H 0.3766699995 3.2572999968 -3.8884499971
C 1.4658599996 3.4287899996 0.5250799998
C 1.9420100004 4.4377199952 -2.1034699995
C 2.5708899998 4.3852899959 0.2692899997
N 2.7126499962 4.8662499951 -1.0224999990
O 3.3265900001 4.7505499971 1.1568299981
O 2.0966900012 4.9068199955 -3.2171899996
C 3.7317799989 5.8903399811 -1.2413500019
H 3.6347099967 6.2310099800 -2.2750799985
H 3.5536899974 6.7223300096 -0.5497799979
H 4.7272799956 5.4583000229 -1.0782499979
O -0.0500200000 1.7479099964 3.3986399959

O -2.2048699995 -0.2692700000 -3.4452499985
C 0.8582800020 2.1827799997 4.4393299957
H 1.2379500013 3.2151199959 4.2711899969
H 1.7190900002 1.4826700016 4.4443099978
C -2.8120700003 -1.0510300008 -4.5029399960
H -2.2365499974 -1.9943299996 -4.5871499972
H -3.8778999975 -1.2987599980 -4.3006699987
C 3.4288599992 0.3059600000 2.8219599995
C 3.9905499980 1.0062499988 1.7815899984
C 3.4830499996 0.8290499993 0.4790599996
C 2.4162600009 -0.0715299998 0.2131799999
C 1.7864699966 -0.7217800006 1.3281800018
C 2.3280800011 -0.5265699998 2.5975299975
H 3.8757899986 0.3915799997 3.8186899998
C 4.0722100001 1.5545600007 -0.5745699975
C 2.0132799995 -0.3147299999 -1.1413199994
H 1.8941899970 -1.0402699972 3.4447900006
C 2.6177299987 0.4520200000 -2.1565399964
C 3.6269699969 1.3850099985 -1.8575200009
H 4.1073699996 1.9586199998 -2.6577899992
C 5.1730399948 2.5180899997 -0.3248499997
C 5.1517599959 1.8893499994 2.0474499985
N 5.6570999935 2.6122899987 0.9673999990
C 6.7598800010 3.5404799986 1.1909999971
H 6.4407600030 4.5544599958 0.9182899992
H 7.0179799929 3.4945599955 2.2517799980
H 7.6191400127 3.2382199993 0.5794500009
O 5.6499700186 3.1964699972 -1.2215100001
O 5.6479099846 1.9757500005 3.1558500001
C 1.0168699980 -1.3749800002 -1.3826200014
C 0.6277099992 -1.6008799983 1.0891699983
C 0.3259199997 -1.9564199985 -0.2647299998
C 0.7358499970 -1.8631400004 -2.6562899988
H 1.2638799968 -1.4591799999 -3.5089499960
C -0.6888900019 -2.9153000009 -0.5299599990
C -0.9349799996 -3.3834599973 -1.8375399999
C -0.1917499999 -2.1270499983 2.1079700008
C -1.2326200015 -3.0230099999 1.8110899979
H -1.8534799975 -3.4372300004 2.6123400007
C -0.2042799997 -2.8735499989 -2.8820700006
H -0.3774000000 -3.2563899972 -3.8892099961
C -1.4659999988 -3.4289400002 0.5244199999
C -1.9422399966 -4.4374799975 -2.1042699990
C -2.5709300003 -4.3855399950 0.2685400000
N -2.7127900006 -4.8662499951 -1.0233200014
O -3.3264999976 -4.7510799998 1.1560800006

O -2.0968300003 -4.9065299958 -3.2180299996
C -3.7317799989 -5.8904599985 -1.2422500001
H -3.6350799974 -6.2305400178 -2.2762099983
H -3.5531699962 -6.7227999719 -0.5512300017
H -4.7272799956 -5.4587299794 -1.0784699981
O 0.0493900000 -1.7475800015 3.3979899969
O 2.2037800003 0.2704299998 -3.4454599972
C -0.8569499998 -2.1847399980 4.4393899991
H -1.7173299992 -1.4841799982 4.4477199998
H -1.2376299973 -3.2164899987 4.2697899950
C 2.8107699971 1.0524600016 -4.5030699990
H 2.2349700013 1.9956200014 -4.5870499986
H 3.8765399962 1.3005300006 -4.3008699960
C -4.7398699998 1.9482699974 -3.2172700006
C -5.5628699902 1.2861800006 -2.3394399964
C -5.5296499913 1.6252299975 -0.9696100017
C -4.6193599979 2.5975500004 -0.4676300000
C -3.7937599959 3.3032399976 -1.4088300004
C -3.8877499962 2.9569200000 -2.7558000001
H -4.7517599978 1.6710000001 -4.2718199982
C -6.4006400096 0.9522499995 -0.0891599999
C -4.5256599972 2.8193099965 0.9477099977
H -3.2631399965 3.4639299963 -3.4779999980
C -5.4552700071 2.1620299982 1.7759599975
C -6.3837800004 1.2480099987 1.2471500011
H -7.0891899940 0.7317799999 1.9072799996
C -7.3423200066 -0.0896699998 -0.5725599972
C -6.4265300045 0.1904899999 -2.8407099969
N -7.3082799947 -0.3926300000 -1.9284499984
C -8.1782399696 -1.4687399990 -2.3985900013
H -9.1382599785 -1.3971199967 -1.8769299987
H -8.3056999733 -1.3557199977 -3.4787799999
H -7.7134799791 -2.4409899970 -2.1818799963
O -8.0974600104 -0.6782399984 0.1815099997
O -6.3728099981 -0.2001299999 -3.9927099989
C -3.4221099999 3.6690200001 1.4418599982
C -2.8311199988 4.3092099981 -0.9157199972
C -2.6105999972 4.3895099989 0.4992599997
C -3.0916799980 3.7550799995 2.7930899961
H -3.6904900000 3.2201599961 3.5172099971
C -1.5440699992 5.1861899955 1.0025599985
C -1.2184500011 5.1994699992 2.3760600012
C -2.0748900011 5.1600199971 -1.7467000010
C -1.0552199995 5.9709200172 -1.2181500000
H -0.4497699999 6.6055000118 -1.8745199986
C -1.9908199990 4.4831499961 3.2568399989

H -1.7317399973 4.4826199987 4.3157600001
C -0.7670499995 5.9613300032 0.1202399998
C -0.0262200000 5.9227899742 2.8785399971
C 0.3838199996 6.7667899970 0.6017600009
N 0.6816399990 6.6984599899 1.9568899978
O 1.0633199986 7.4406799735 -0.1531499998
O 0.3383300001 5.8414399853 4.0372899983
C 1.8621999965 7.4258199895 2.4185499994
H 1.8079700009 7.4957400153 3.5083499990
H 2.7702300011 6.8795999942 2.1264299984
H 1.8711899976 8.4198600074 1.9582300015
O -2.3483199975 5.1716499997 -3.0873900007
O -5.4623399733 2.4436999982 3.1175799997
C -1.5278700009 5.9712100063 -3.9718299997
H -1.1270299975 6.8860699794 -3.4838600006
H -0.6737199995 5.3407499737 -4.2901099977
C -6.0500600033 1.4772300017 4.0238099974
H -7.0088199884 1.0676699993 3.6382999984
H -5.3284799947 0.6352199975 4.1460199970
C 4.7392699975 -1.9470799996 -3.2182099992
C 5.5624799866 -1.2852799971 -2.3403500013
C 5.5295299739 -1.6247400006 -0.9706099985
C 4.6192999998 -2.5971599968 -0.4687400000
C 3.7935399957 -3.3025899986 -1.4099799977
C 3.8872499978 -2.9558799975 -2.7568699964
H 4.7509299992 -1.6694499977 -4.2726699997
C 6.4007200212 -0.9520499969 -0.0901199999
C 4.5258099978 -2.8192899989 0.9465600004
H 3.2624899975 -3.4626899965 -3.4790799958
C 5.4556200049 -2.1623099965 1.7748299977
C 6.3841099953 -1.2482199974 1.2460999971
H 7.0896900135 -0.7322399977 1.9062399971
C 7.3423600124 0.0899699999 -0.5734099987
C 6.4259699763 -0.1893600001 -2.8414199992
N 7.3078199810 0.3935699997 -1.9291399979
C 8.1776399885 1.4698399996 -2.3991700007
H 9.1376599974 1.3982899969 -1.8774900004
H 8.3051600008 1.3569299985 -3.4793699955
H 7.7127699820 2.4420299996 -2.1824099990
O 8.0978000067 0.6781500012 0.1806800001
O 6.3719899851 0.2016199999 -3.9932799968
C 3.4222799981 -3.6690299962 1.4406700003
C 2.8310200002 -4.3087199959 -0.9169599970
C 2.6106399977 -4.3892899988 0.4980099995
C 3.0919699977 -3.7553199972 2.7919099997
H 3.6908999959 -3.2205999963 3.5160899988

C 1.5441600016 -5.1860599978 1.0012499992
C 1.2185799988 -5.1994699992 2.3747599980
C 2.0747999986 -5.1594499991 -1.7480299979
C 1.0552499985 -5.9705300136 -1.2195299989
H 0.4498499998 -6.6051100082 -1.8759600010
C 1.9910299977 -4.4833199996 3.2555999992
H 1.7319599974 -4.4828399988 4.3145399980
C 0.7671400019 -5.9611399757 0.1188800001
C 0.0262600000 -5.9227100155 2.8771499967
C -0.3835799998 -6.7668300028 0.6003899981
N -0.6813700022 -6.6986100117 1.9555299965
O -1.0629199988 -7.4408900039 -0.1545299997
O -0.3385600001 -5.8410899875 4.0357999993
C -1.8616800005 -7.4263200091 2.4172800005
H -1.8071099980 -7.4966699913 3.5070399996
H -2.7699199985 -6.8801699710 2.1257099999
H -1.8706499987 -8.4201699994 1.9565500014
O 2.3481899998 -5.1708899954 -3.0887199977
O 5.4629200045 -2.4443899976 3.1163599975
C 1.5274099978 -5.9700199926 -3.9732399977
H 1.1269299989 -6.8851800091 -3.4855599982
H 0.6730099971 -5.3395000042 -4.2907699981
C 6.0507399960 -1.4781599989 4.0227799963
H 7.0093200079 -1.0683000006 3.6371800001
H 5.3290300215 -0.6363299996 4.1454799981
C -6.2605899805 2.1711400008 5.2710299981
C -6.4435099782 2.7286199981 6.3073599852
H -6.6102700152 3.2265299985 7.2338400018
C -2.3619199999 6.3265500145 -5.0949799959
C -3.0371999979 6.6283099837 -6.0283199748
H -3.6405400002 6.9007699930 -6.8625700133
C -2.6964399965 -0.2624100001 -5.7064199973
C -2.6128199962 0.3712899999 -6.7113100001
H -2.5421799983 0.9349999972 -7.6120699935
C 0.1185400000 2.1141699997 5.6766200178
C -0.4741799999 2.0688499989 6.7085699734
H -1.0010699995 2.0318700001 7.6332899996
C -0.1147699998 -2.1193899995 5.6754100012
C 0.4799499995 -2.0768499993 6.7063300192
H 1.0085899993 -2.0423599964 7.6301500208
C 2.6953199983 0.2639400001 -5.7066299748
C 2.6118899990 -0.3696599996 -6.7115999892
H 2.5414199993 -0.9331799981 -7.6125000029
C 6.2617199856 -2.1724900007 5.2696899996
C 6.4449799796 -2.7303099996 6.3057800208
H 6.6121499702 -3.2284999982 7.2320400055

C 2.3609800012 -6.3246199994 -5.0969699985
C 3.0358599995 -6.6257799875 -6.0308000167
H 3.6388699963 -6.8977199744 -6.8654600088

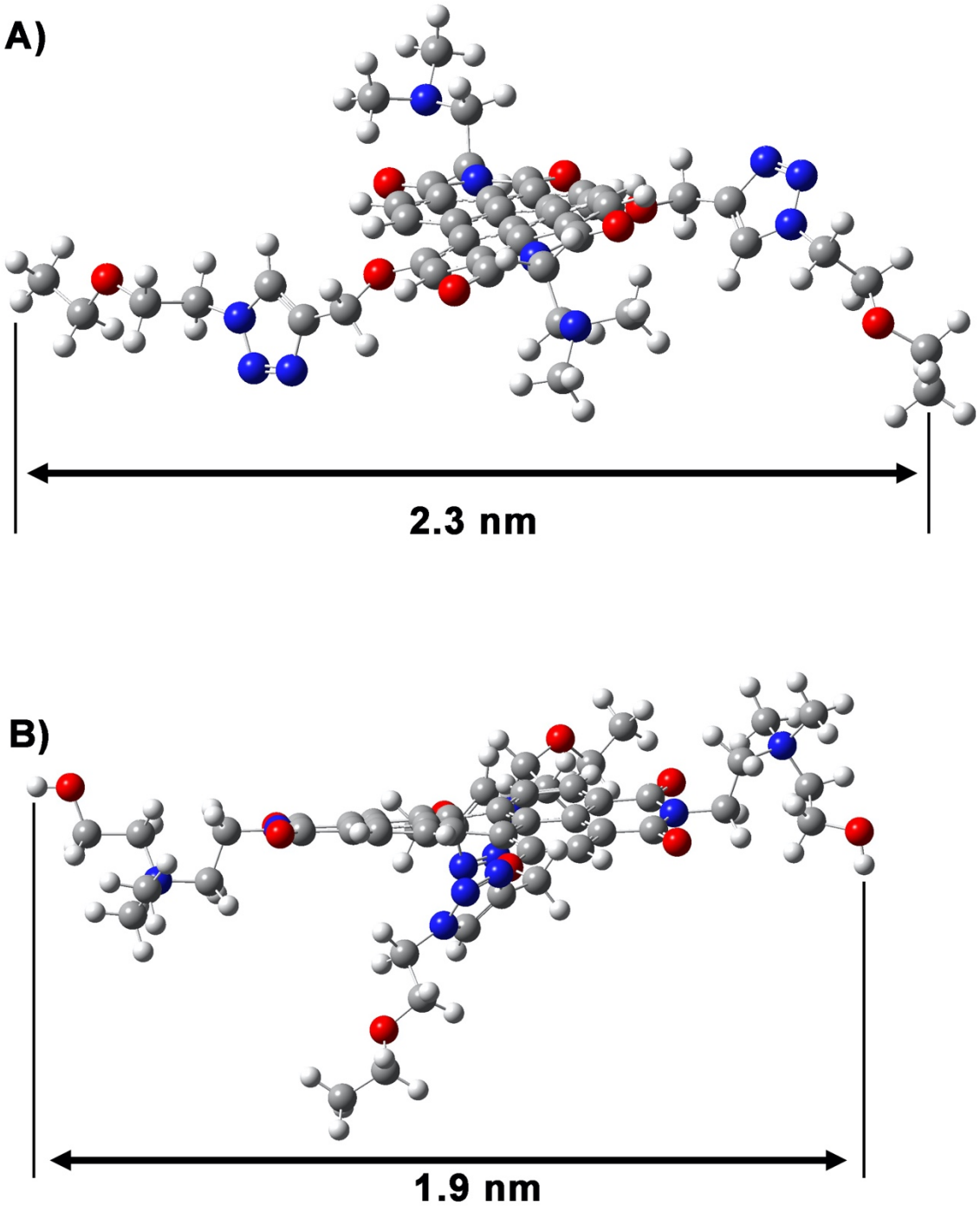

Figure S31: Energy-minimized structure of a model **PBI-OC$_1$-Stap-n** unit that highlights the length of the side chains along bay-functionalized axis (A) and the diimide axis(B).

10. ^{1}H NMR, ^{13}C NMR, and IR Spectra (p. 45-57)

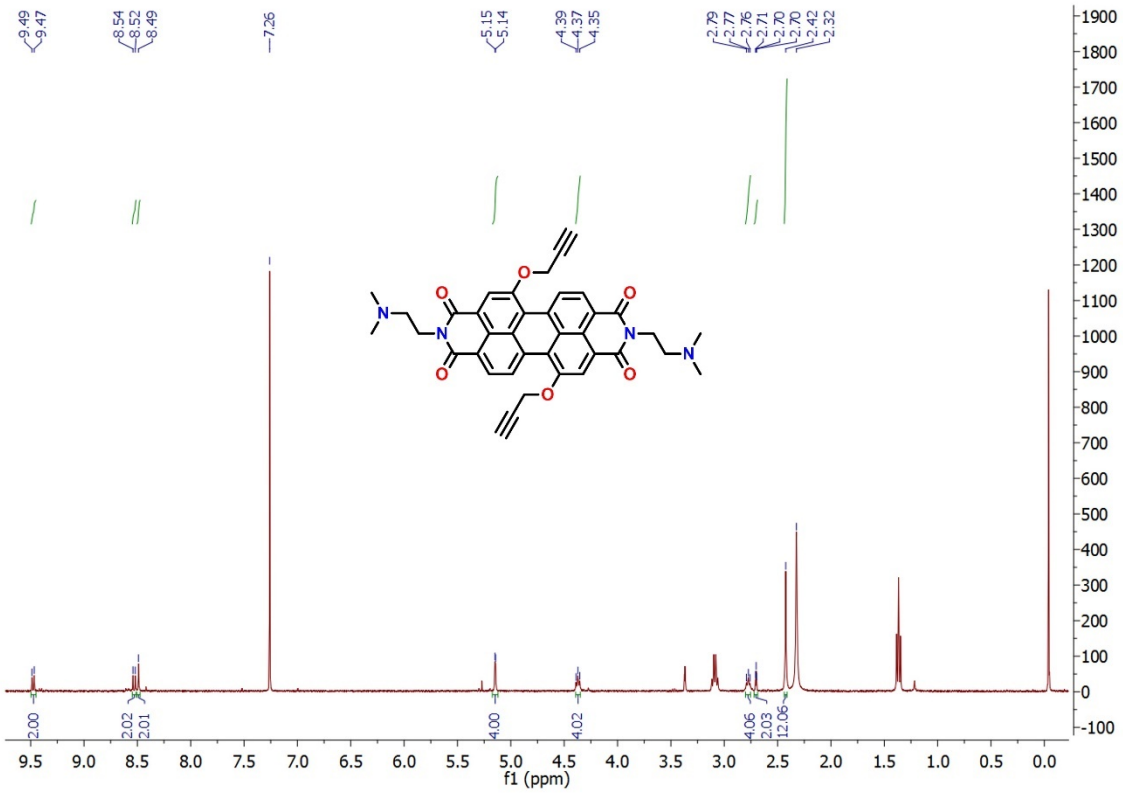

Figure S32. ^{1}H NMR spectrum (400 MHz, $CDCl_3$, 298 K) of **PBI-OC$_1$C≡CH-NMe$_2$**.

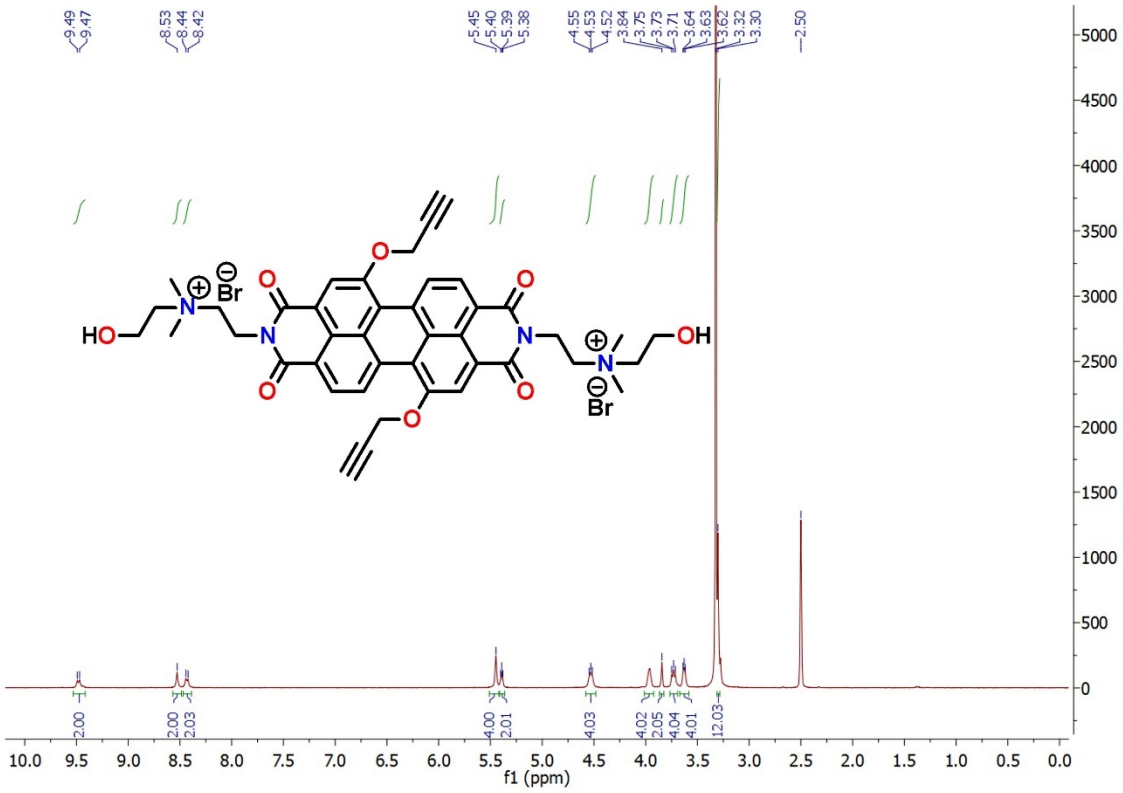

Figure S33. ^{1}H NMR spectrum (400 MHz, *d*$_6$-DMSO, 298 K) of **PBI-OC$_1$C≡CH**.

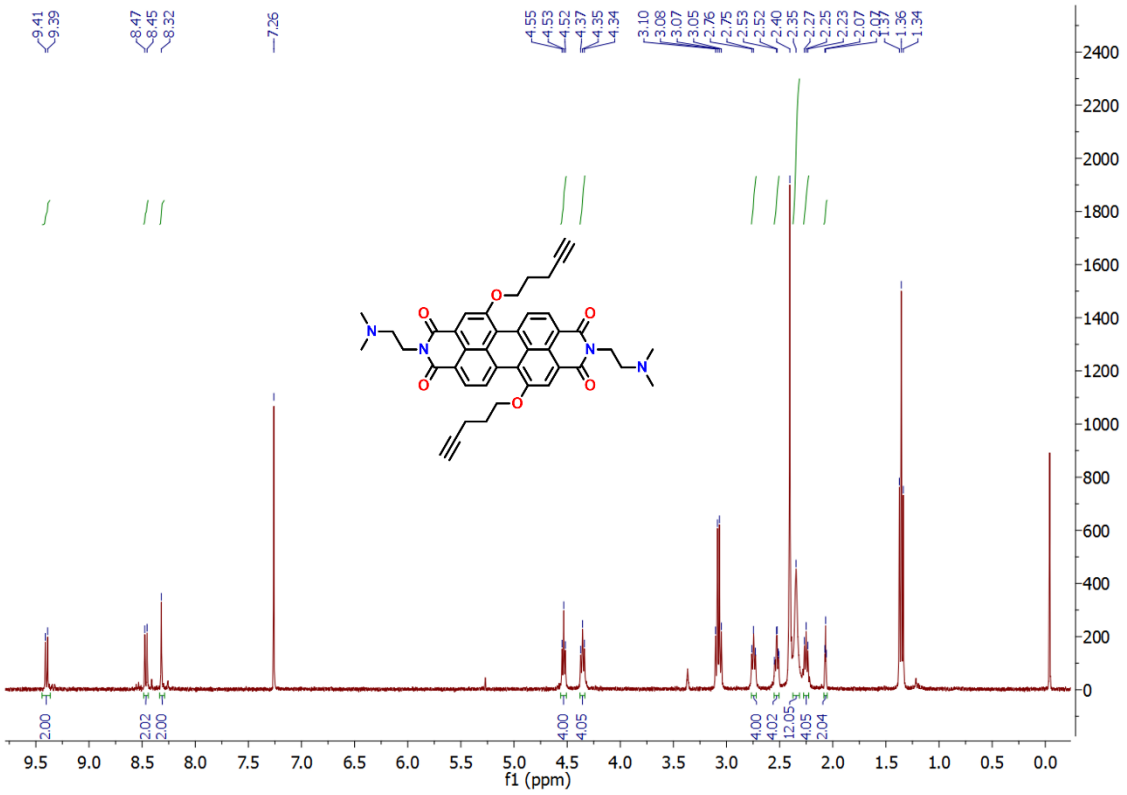

Figure S34. ^{1}H NMR spectrum (400 MHz, $CDCl_3$, 298 K) of **PBI-OC$_3$C≡CH-NMe$_2$**.

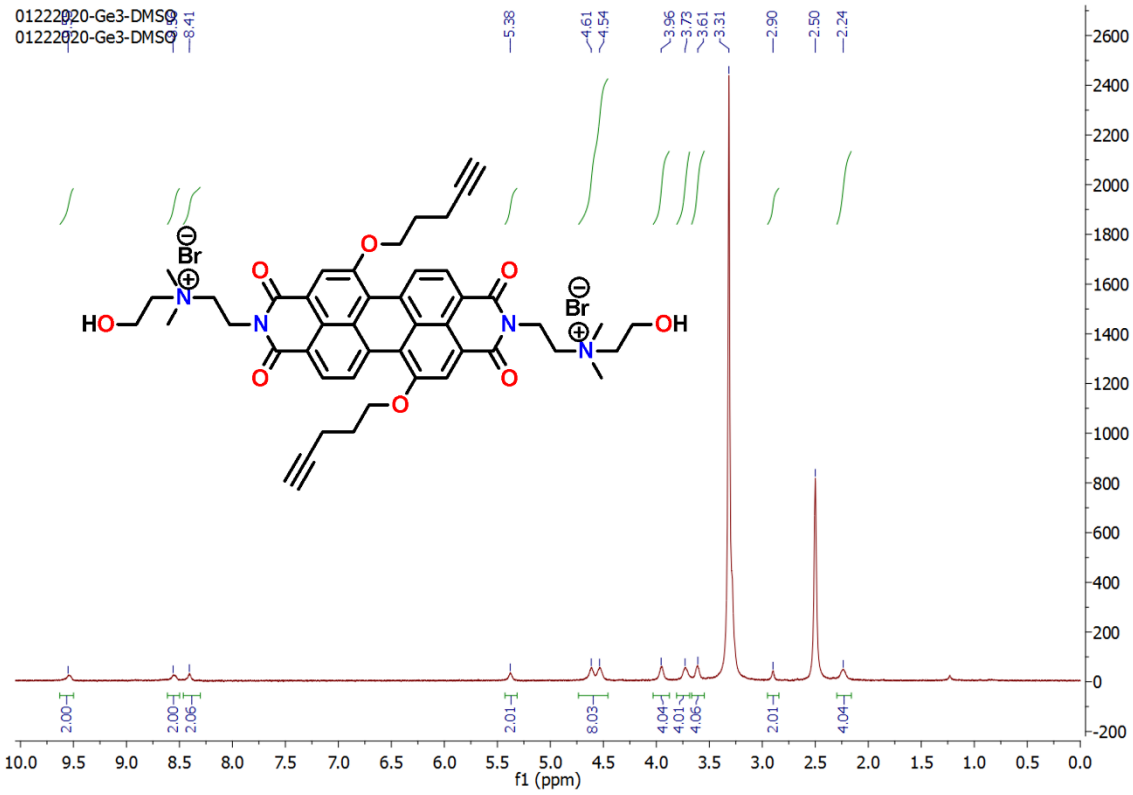

Figure S35. ^{1}H NMR spectrum (400 MHz, d_6-DMSO, 298 K) of **PBI-OC$_3$C≡CH**.

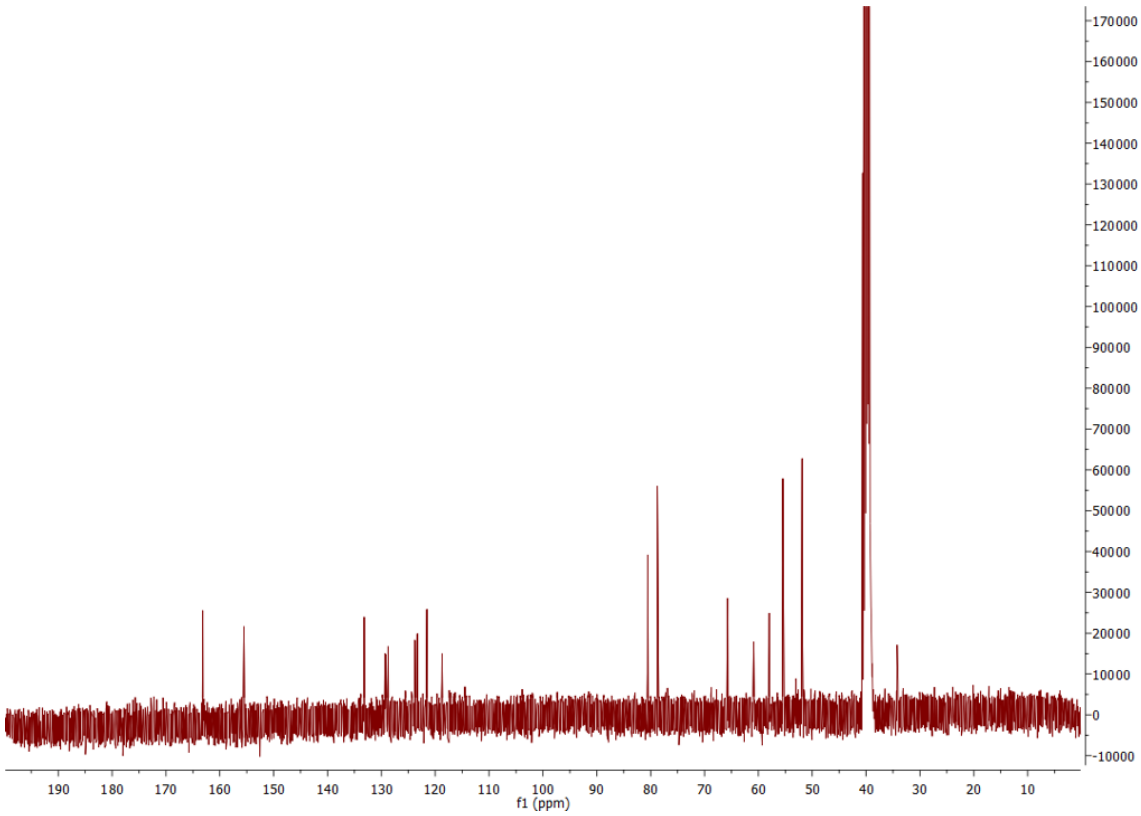

Figure S36. ^{13}C NMR spectrum (101 MHz, d_6-DMSO, 298 K) of **PBI-OC$_1$C≡CH-NMe$_2$**.

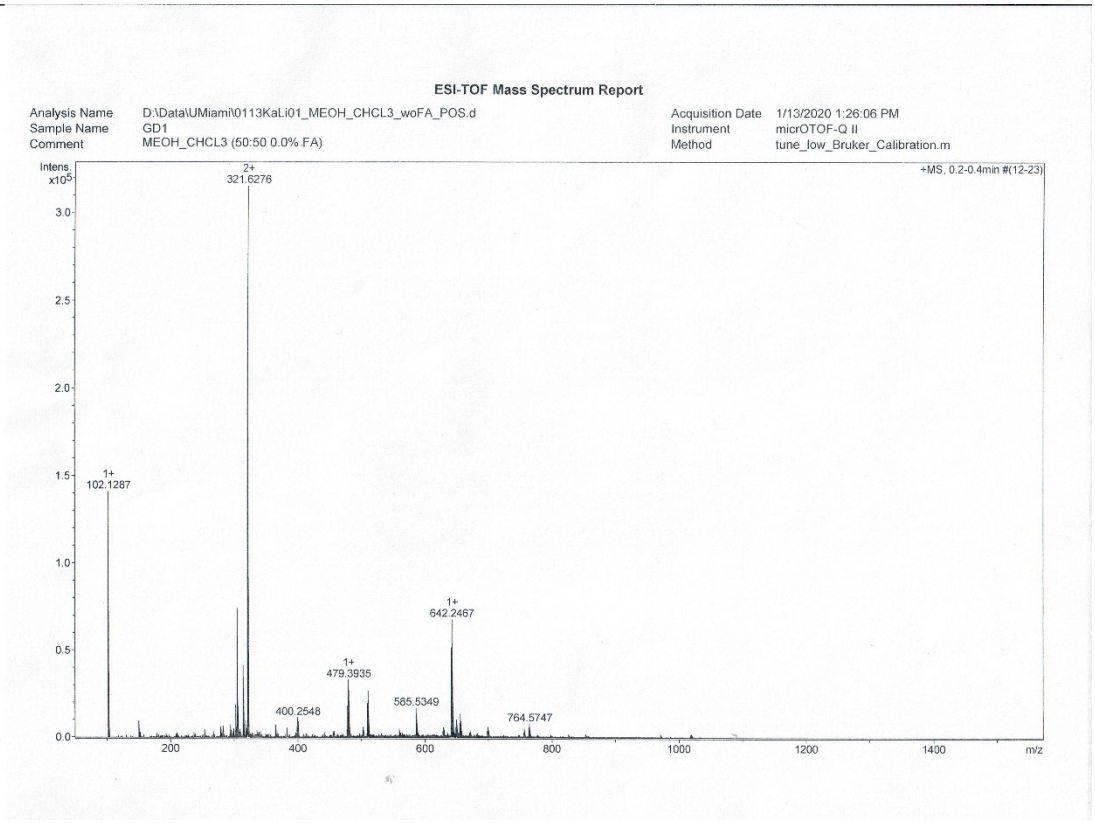

Figure S37. High-resolution mass spectrum of **PBI-OC$_1$C≡CH-NMe2**.

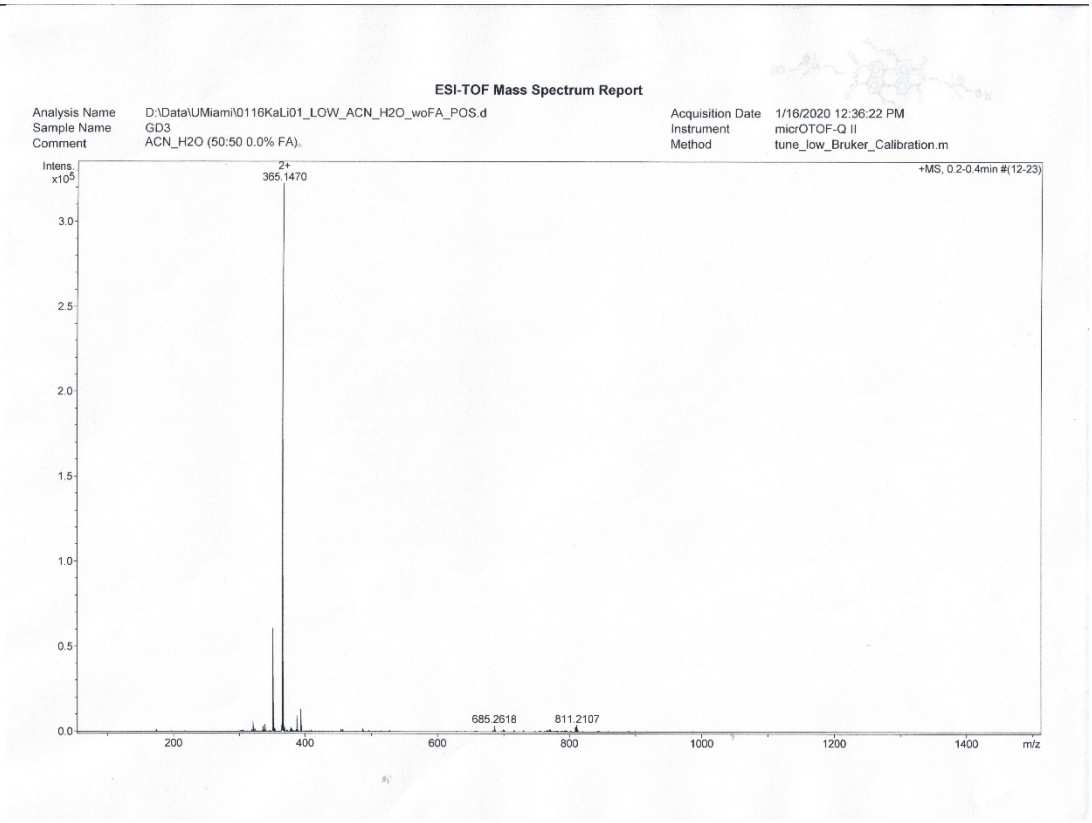

Figure S38. High-resolution mass spectrum of **PBI-OC$_1$C≡CH**.

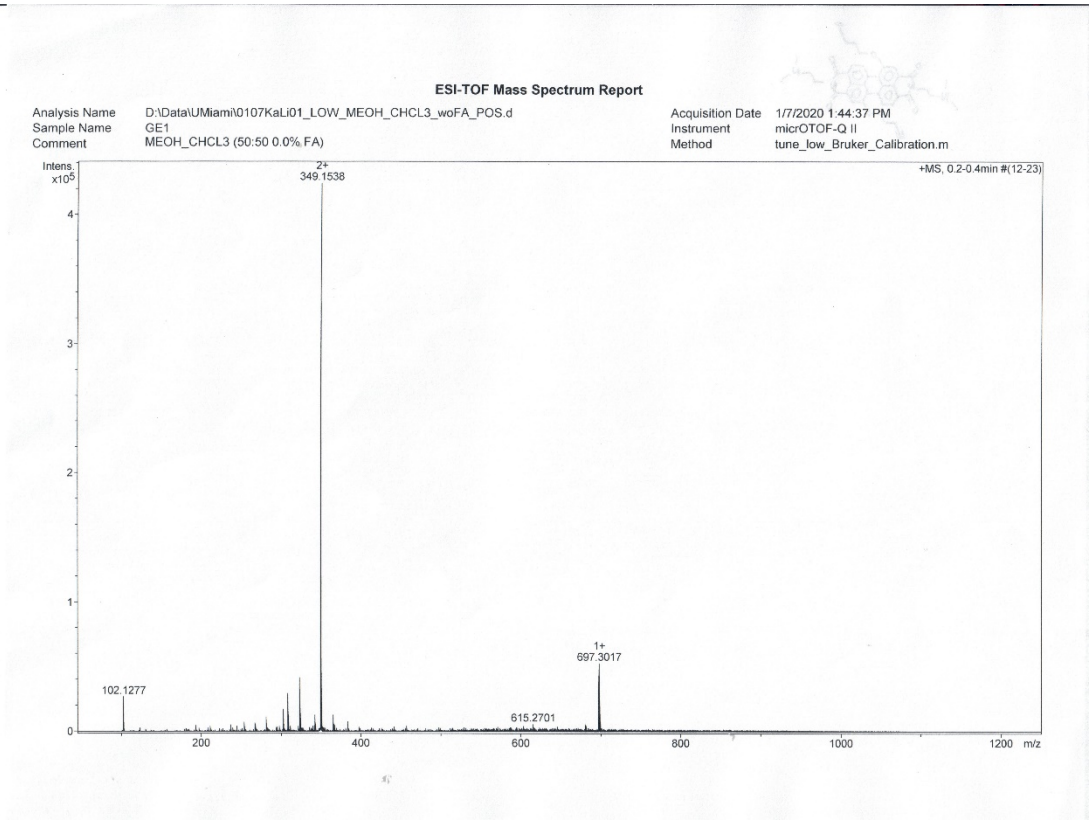

Figure S39. High-resolution mass spectrum of **PBI-OC$_3$C≡CH-NMe$_2$**.

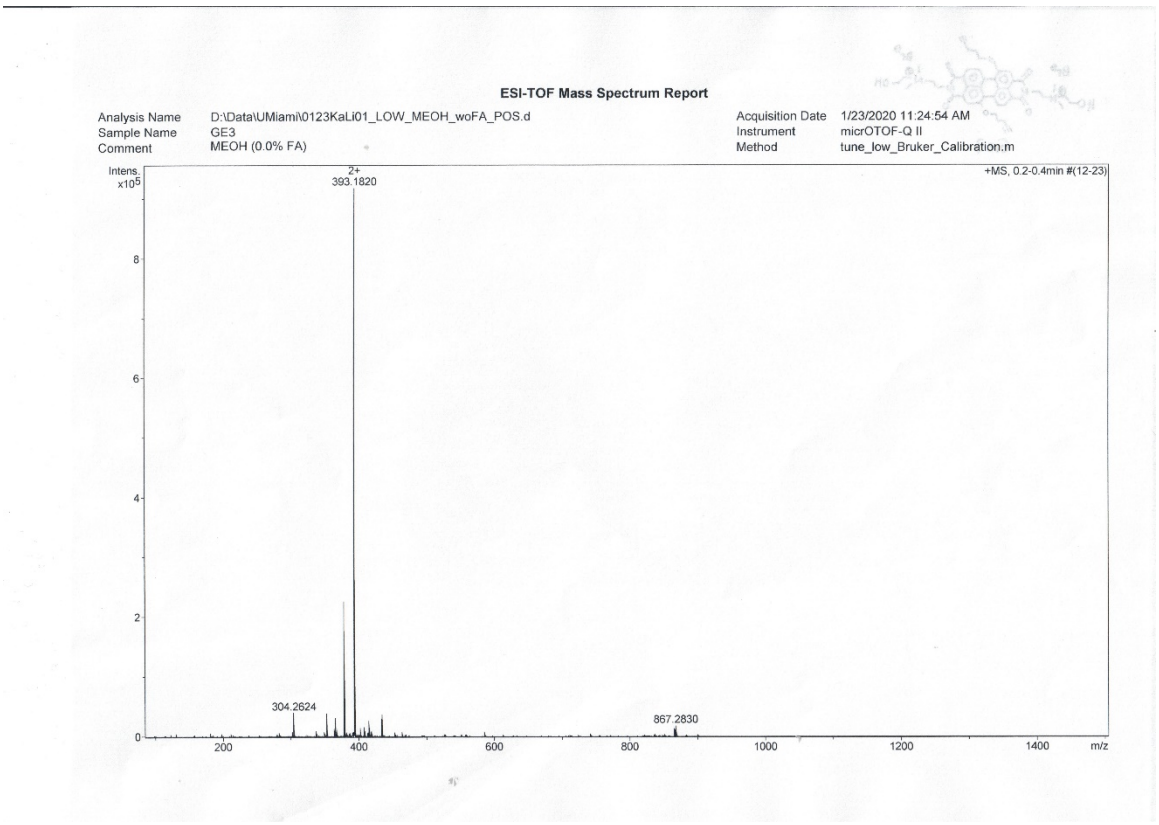

Figure S40. High-resolution mass spectrum of **PBI-OC$_3$C≡CH**.

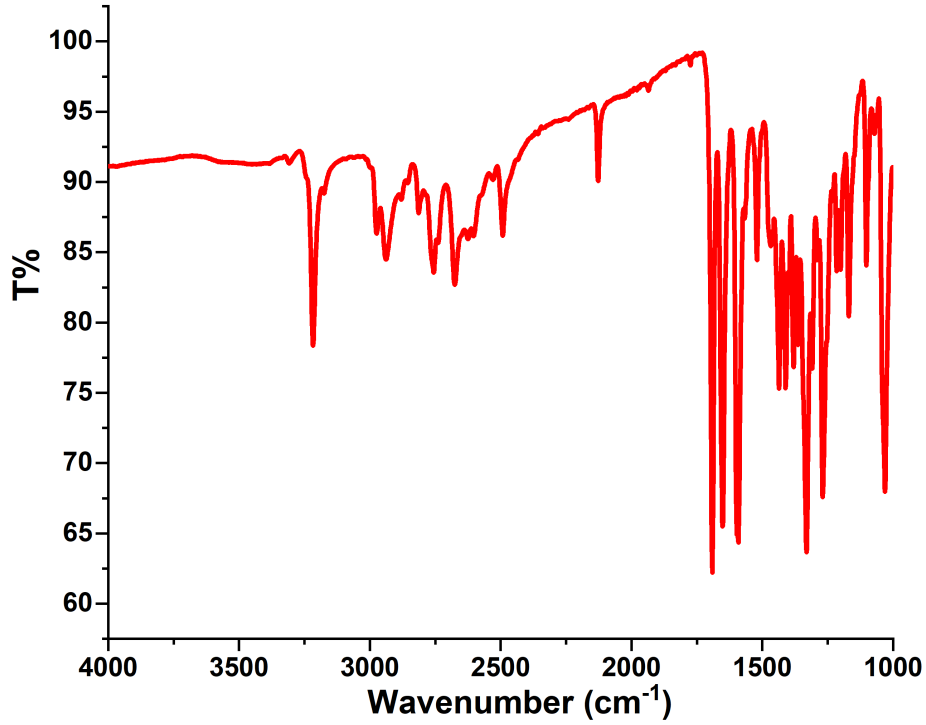

Figure S41. FTIR spectrum (neat solid) of **PBI-OC$_1$C≡CH-NMe$_2$**.

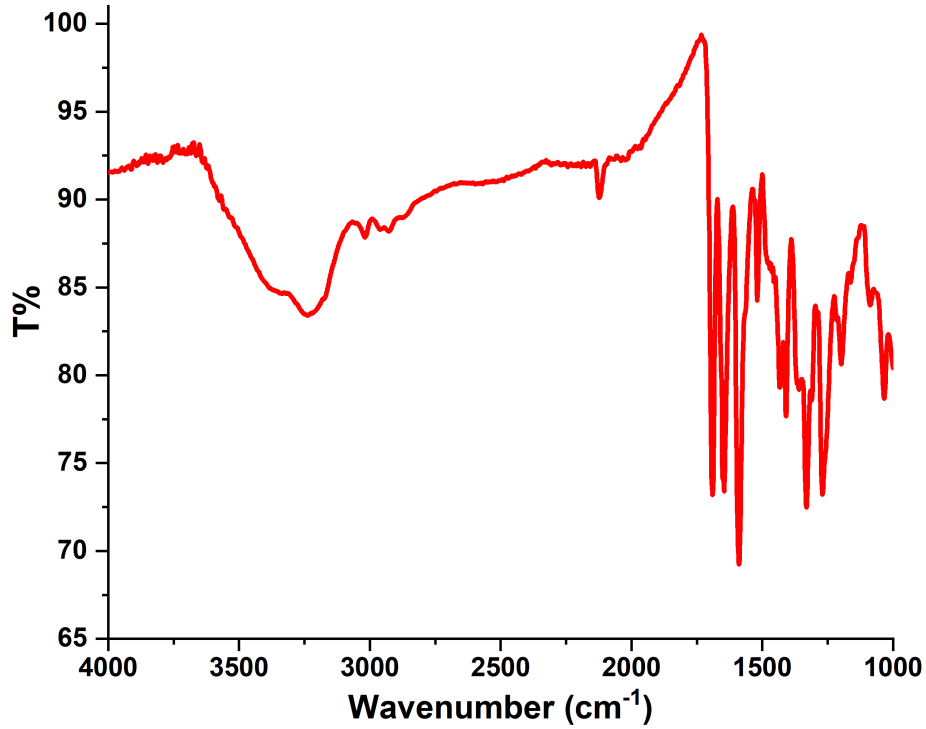

Figure S42. FTIR spectrum (neat solid) of **PBI-OC$_1$C≡CH**.

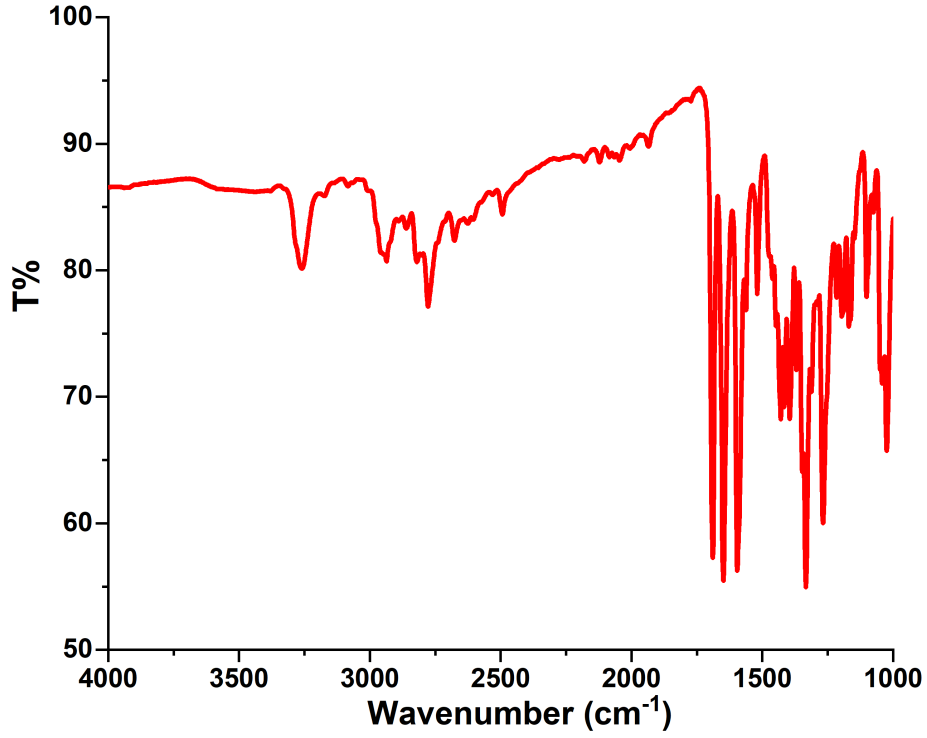

Figure S43. FTIR spectrum (neat solid) of **PBI-OC$_3$C≡CH-NMe$_2$**.

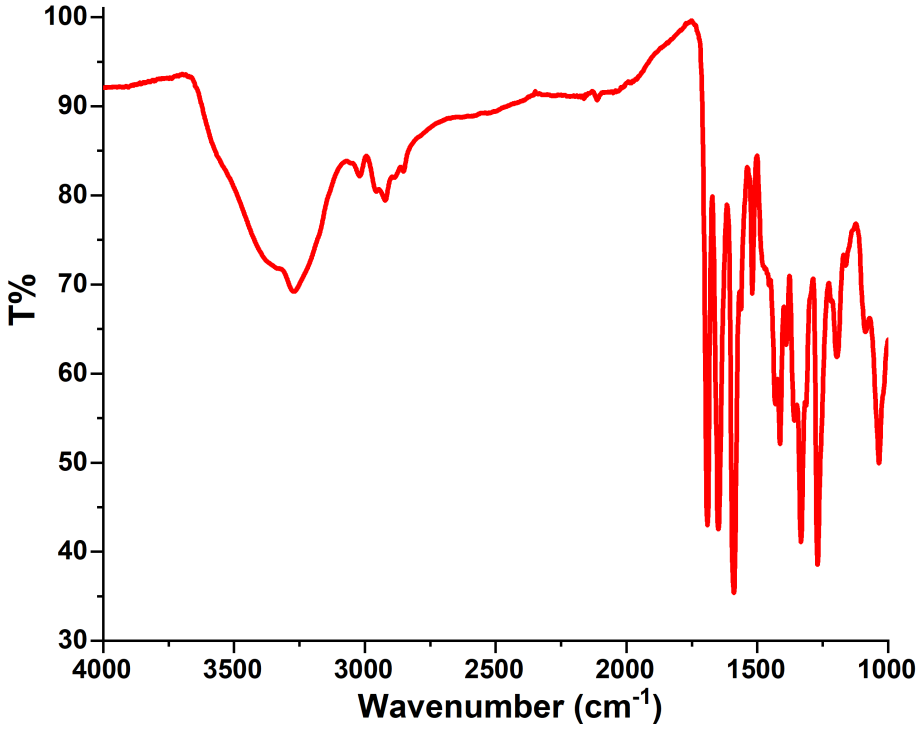

Figure S44. FTIR spectrum (neat solid) of **PBI-OC$_3$C≡CH**.

11.References

1. Würthner, F.; Stepanenko, V.; Chen, Z.; Saha-Möller, C. R.; Kocher, N.; Stalke, D., *J. Org. Chem.* **2004,** *69*, 7933-7939.
2. Ashcraft, A.; Liu, K.; Mukhopadhyay, A.; Paulino, V.; Liu, C.; Bernard, B.; Husainy, D.; Phan, T.; Olivier, J. H., *Angew. Chem. Int. Ed.* **2020,** *59*, 7487-7493.
3. Narita, S.; Kobayashi, N.; Mori, K.; Sakurai, K., *Bioorg. Med. Chem.* **2019,** *29*, 126768.
4. Smulders, M. M. J.; Nieuwenhuizen, M. M. L.; de Greef, T. F. A.; van der Schoot, P.; Schenning, A. P. H. J.; Meijer, E. W., *Eur. J. Chem.* **2010,** *16*, 362-367.
5. Paulino, V.; Cadena, D. M.; Liu, K.; Mukhopadhyay, A.; Roberts, S. T.; Olivier, J.-H., *Chem. Mater.* **2022,** *34*, 6518-6528.
6. Spano, F. C., *Chem. Phys.* **2006,** *325*, 22-35.
7. Spano, F. C.; Silva, C., *Annu. Rev. Phys. Chem.* **2014,** *65*, 477-500.
8. Williams, A. T. R.; Winfield, S. A.; Miller, J. N., *Analyst* **1983,** *108*, 1067-1071.
9. Rurack, K., Fluorescence Quantum Yields: Methods of Determination and Standards. In *Standardization and Quality Assurance in Fluorescence Measurements I: Techniques*, Resch-Genger, U., Ed. Springer Berlin Heidelberg: Berlin, Heidelberg, 2008; pp 101-145.